CERN 70-12
Nuclear Physics Division
23 April 1970

ORGANISATION EUROPÉENNE POUR LA RECHERCHE NUCLÉAIRE
CERN EUROPEAN ORGANIZATION FOR NUCLEAR RESEARCH

HIGH-ENERGY PARTICLE SPECTRA FROM PROTON INTERACTIONS AT 19.2 GeV/c

J.V. Allaby, F. Binon*), A.N. Diddens, P. Duteil, A. Klovning, R. Meunier**), J.P. Peigneux***), E.J. Sacharidis†), K. Schlüpmann, M. Spighel††), J.P. Stroot*††), A.M. Thorndike†††) and A.M. Wetherell

GENEVA
1970

*) Visitor from Institut Interuniversitaire des Sciences Nucléaires, Bruxelles.

**) Visitor from CEN, Saclay.

***) Visitor from Université de Clermont-Ferrand.

†) Present address: Rutherford High Energy Lab., Chilton, Berks.

††) IPN, Faculté des sciences, Orsay.

†††) Visitor from Brookhaven National Laboratory, Upton, L.I., N.Y.

1. INTRODUCTION

Several studies[1-7] of particle production in high-energy proton collisions, above 10 GeV, have been made in the past few years using both proton and nuclear targets. While a considerable number of cross-sections have been measured and some general features of the production processes established it has been clear that much more experimental data would be needed to examine more deeply the reaction mechanisms involved. One of the best established features of secondary production at high energies is that the particles are restricted to a forward cone characterised by an average-transverse momentum, p_T, of about 400 MeV/c. The aim of the present experiment was to produce a rather dense set of data points within this region for both hydrogen and nuclear targets. Furthermore the intention was to provide information up to the highest possible secondary momenta for all of the types of particles, since such data has not, up to now, been available.

The scope of the results from this experiment may be summarized briefly as follows:

(1) Proton-proton interactions at 19.2 GeV/c; production cross-sections for positive and negative pions and kaons, protons and anti-protons. Measurements were made at laboratory angles of 12.5, 20, 30, 40, 50, 60 and 70 mrad for momenta of 4.5, 6, 8, 10, 11, 12, 13 and 14 GeV/c. At the smallest angles momentum scans in small steps of about 70 MeV/c were made for all of the particles, from 14 GeV/c up to the highest possible momenta, or to where the cross-section $d^2\sigma/d\Omega dP$ falls below 10^{-32} cm^2/sr.GeV/c in the laboratory system.

(2) Proton-nuclear interactions at 19.2 GeV/c; the targets used were B_4C, Be, Al, Cu and Pb. The same angular range as for hydrogen was covered at momenta of 6, 7, 10, 12 and 14 GeV/c for the negatively charged particles and 6, 8, 10, 12, 14 and 16 GeV/c for the positives. In addition, fine momentum scans at the smallest angle and up to the highest momenta were made for both negatives and positives produced on Be and Al.

In this report a short description of the spectrometer used in this experiment is given (section 2) and the data will be presented in the form of a table of cross-sections and various graphical representations (sections 3 and 4). Some of the data have been presented at the Vienna Conference (1968).

Several other experiments have been performed with this spectrometer. The results have been published: elastic proton scattering[8a], isobar production[8b], $pp \to D\pi$ and $pp \to D\rho$[8c] and proton-deuteron scattering[8d].

2. EXPERIMENTAL METHOD

The experimental layout is shown in Fig. 1. A long pulse extracted proton beam ($\sim 3 \cdot 10^{11}$ proton pulse, $\sim$ 100 ms pulse length, $\Delta p/p \simeq 10^{-3}$) was used to bombard a 10 cm long, 4 cm diameter helium-cocled liquid hydrogen target[9] or nuclear targets with surface densties of about 1 gm cm^{-2}. At the target the beam had a diameter of about 5 mm and a divergence of about 0.5 mrad in both the horizontal and in the vertical planes. The position and size of the beam were monitored by use of a fluorescent screen which could be moved into it just ahead of the target.

The charged particles produced in the target were momentum analysed and detected in a single arm spectrometer of high resolution. A ray diagram for the arrangement is given in Fig. 2. The quadrupole doublet Q_1 and Q_2 focused particles at the dispersive focus F_1, the dispersion of 0.7% per cm being provided by the momentum analysis of three 2-metre long dipole magnets M_3, M_4 and M_5. The latter were connected in series to a common power supply and produced a deflection of 120 mrad. The quadrupole doublet Q_6 and Q_7 produced an achromatically compensated focus at F_2. Dispersion compensation was achieved by the 6 m long dipole magnet M_6 and the symmetric triplet Q_3, Q_4 and Q_5. A quadrupole doublet with F_2 as its focus finally rendered the particle beam parallel. The magnetic fields of the dipoles M_5 and M_6 were continuously monitored by nuclear resonance equipment.

The production angle of the particles accepted by the spectrometer could be varied by means of the magnet M_1 which was a septum type

window frame magnet (aperture 10 x 6 (H x V) cm^2, length 2.5 m, maximum magnetic field 14.5 kG) with a narrow coil 3.5 cm wide on the side adjacent to the primary proton beam. M_1 could be displaced by remote control in order to accept particles emitted in the interval 12.5 to 70 mrad. The magnet M_2 was a 1 metre long C magnet fixed on the axis of the spectrometer. The deflecting strengths of the magnets M_1 and M_2 were chosen so that the particles accepted at a particular angle by M_1 followed the spectrometer axis after leaving M_2. The magnetic properties of all the dipole elements of the spectrometer were determined to ~ 0.1% by the floating wire method.

The linear magnification in the spectrometer was about one half in the horizontal and in the vertical planes both at F_1 and F_2. A scintillator, S, 25 mm wide and 17.5 mm high was placed at F_2 accepting the whole particle flux transmitted by the spectrometer. At the dispersive focus, F_1, 5 scintillators A_i (i = 1, ... 5) 15 mm high were placed side by side to cover a width of 30 mm giving a momentum acceptance $\Delta p/p = 2.1\%$. The counters A_i and S were mounted on remotely controlled moveable supports, so that the particle distributions at the foci could be checked by scanning the counters through the images of the target.

The acceptance in solid angle was determined by a circular collimator placed in the quadrupole Q_2. The collimator size could be varied to limit the particle flux to a convenient level. The biggest aperture (8 cm diameter) was normally used. It corresponded to a horizontal acceptance of about 2 mrad and a vertical acceptance of about 5 mrad, giving a solid angle $\Delta\Omega = 7.62 \times 10^{-6}$ sr. The effective momentum resolution of the spectrometer, as given by the full width at half height of the p-p elastic scattering momentum peak at the smallest scattering angles, was about 0.5%.
At the largest production angle, however, the momentum resolution deteriorated somewhat due to the increase in source size because of the finite length of the target. After magnetic calibration of the spectrometer by the floating wire technique and momentum calibration using elastically scattered protons it was found that the instrument behaved essentially as expected from trajectory calculations using

a standard computer programme. At each setting of angle and momentum however, one precaution was taken namely to check the excitation of the steering magnet M_1 by plateauing it with respect to the counting rate of the coincidence A_3S.

Particle identification was performed by a system of gas Čerenkov counters consisting of three threshold counters[10] C_1, C_2 and C_3 and a differential counter, DISC[11]. Two 10 cm diameter counters D_1 and D_2 were placed just before and just after the DISC in order to define the beam within the counter. The three threshold Čerenkov counters in various combinations of coincidence and anti-coincidence together with the coincident signals from the counters S and D_1 and D_2 were generally sufficient to distinguish the various particles. At the high-energy end of the momentum spectra, however, it was often necessary to introduce a signature from the DISC counter to obtain a clean identification. The momentum spectra of up to three kinds of particles could be measured simultaneously by using three different identification signals to gate the five momentum ladder counters A_i.

The proton beam flux was monitored by a secondary emission chamber[12] placed about 2 m ahead of the hydrogen target. Two triple coincidence counter telescopes, F and M, detecting secondary particles emitted from the target at 9^o and at 90^o, respectively were used for relative monitoring of the beam intensity. The secondary emission chamber and the counter telescopes were calibrated absolutely by measuring the ^{24}Na activity produced in thin Al foils placed in the beam behind the secondary emission chamber. An activation cross section of 8.6 ± 0.5 mb was assumed[13].

3. RESULTS ON HYDROGEN

3a) Laboratory Spectra

The experimental data were corrected for the following effects:

(1) Empty target background which was generally about 20%.

(2) Decay of unstable particles along the spectrometer.

(3) Absorption of the particles along the beam. This was minimised by transporting the particles wherever possible in vacuum and was of the order of 10%.

(4) Loss of particles in the DISC and D_1, D_2 counters, because the aperture of the DISC was slightly limiting the acceptance of the largest collimator settings. The loss was measured at every spectrometer setting and was usually not more than about 10%.

(5) Deadtime of the electronic circuits. This was kept, by limiting the flux, always smaller than about 5%.

(6) The detection efficiency of the DISC in those cases where the DISC was used. This efficiency was carefully measured and was about 70% for pions and kaons.

The cross-sections thus obtained are listed in Table 1 and shown in Figures 3 to 8.

The percentage error quoted after each cross-section is the point to point error, since it is composed of the contributions of the statistical error, of short-term monitor fluctuations and of the variation in the corrections for small changes in momentum and angle. The two latter contributions were usually ± 3 to $\pm 5\%$. The reproducibility of the measurements spaced by a long time interval was usually within 10%. The scale error is about $\pm 10\%$, arising mainly from the uncertainty in the ^{24}Na production cross-section used for the absolute calibration of the monitors and partly from the estimated error in the solid angle and momentum acceptance calculations and from the overall error in the corrections applied. Thus the overall absolute error is about $\pm 15\%$, to be added to the point to point error of Table 1.

The values plotted in Figs. 3-8 are the laboratory cross-sections, $d^2\sigma/d\Omega dP$, with as abscissa the secondary particle momentum

P, for various production angles. The arrow indicates the maximum momentum which the relevant particle can acquire in a proton + proton collision at 19.20 GeV/c, at 12.5 mrad production angle, assuming the usual conservation laws of charge, baryon number and strangeness. The values are collected in Table 2.

The Figures 3-8 are recapitulated in Fig. 9 on a smaller scale, for a better comparison.

The curves for 12.5 mrad production angle for all six particles are redrawn in Fig. 10. This graph demonstrates clearly the different high momentum behaviour of the secondary particles: the proton cross-section increases with increasing momentum, the positive meson cross-sections stay relatively large until they approach their kinematic limit, the π^- spectrum decreases rather smoothly, although quite steeply finally, and the K^- and $\bar{p}$ spectra fall monotonically.

3b) The Structures in the π^+- Spectrum

The π^+ spectra, Fig. 4, show some structure. This phenomenon will now be discussed in more detail.

The spectrum at 12.5 mrad production angle, and to a lesser extent the one at 20 mrad, shows three bumps. The one at the kinematic limit of the spectrum, 17.8 GeV/c, is a peak due to the two-body reaction $p + p \rightarrow \pi^+ + d$. The angular distribution of this reaction has been measured by detecting the deuteron and the results are presented in another communication[8c].

At 6 GeV/c momentum there seems to be another peak. The evidence from the present data alone is poor, as it is based on only one point. The lines connecting the points are therefore dashed in this momentum region. However, the same phenomenon is seen in the small angle π^+ data of Anderson et al[5] and in the 0^o data of Dekkers et al.[3] An explanation might be that these pions originate from $N^*(1238)$ decay. This nucleon isobar is known to be produced very peripherally. The maximum momentum of a pion, originating in $N^*(1238)$ decay is about 8 GeV/c, but the peak in the momentum distribution will be at a somewhat lower momentum.

The third bump can be distinguished in the momentum region of 15 to 16 GeV/c. Its explanation is not so straightforward. In Fig. 11 the high-energy part of the same spectrum is presented with the π^+ missing mass as abscissa. This shows the deuteron peak, followed by a smooth curve, which however shows an excess of events at a two-baryon mass of 2.67 GeV, with a width of 200 MeV. In the 20 mrad data the phenomenon is present, but less pronounced. A possible interpretation could be that two baryons not only form a bound state at the deuteron mass, but also a resonance at 2.67 GeV. This state would have isospin 0 or 1, since there is no similar structure in the π^- spectrum. The angular distribution of the process in which this state is formed is strongly peaked forward, like the angular distribution of the deuteron. It is perhaps worth noting that a mass of 2.67 GeV is very near to the sum of the mass of the $N^*(1688)$ and the nucleon.

George et al[14] found in p + p total cross section measurements a small deviation from a smooth curve at a dibaryon mass of 2.75 GeV. If this is the same effect as noticed in the present experiment, then this would support an isospin 1 assignment.

In a similar experiment at 12.5 GeV (where however the backward produced π^+ was detected instead of the forward produced one), Lamb et al[15] found an excess of backward produced π^+ which could indicate production of a dibaryon at about the same mass. They suggested an alternative interpretation in terms of production and decay of single baryon resonances. Such an explanation cannot be excluded for the present experiment either, but it is remarkable that the excess of π^+ produced in both experiments corresponds to about the same dibaryon mass.

3c) Centre of Momentum Spectra

The laboratory cross sections have been converted to the centre of momentum (C.M.) system. Fig. 12 shows the range in the variables $\bar{p}_L$ and $\bar{p}_T$, the longitudinal and transverse C.M. momenta, that have been covered in the present experiment. The figure is actually relevant to the case where the secondary particle detected is a proton but the other 5 cases are rather similar.

In the next six figures the double differential cross-section per volume element in the C.M. momentum space

$$X = \frac{d^2\sigma}{2\pi\, \bar{p}_T\, d\bar{p}_T\, d\bar{p}_L} = \frac{1}{\bar{p}^2}\,\frac{d^2\sigma}{d\bar{\Omega} d\bar{p}}$$

has been plotted as a function of $\bar{p}_L$ for constant $\bar{p}_T$ (left hand side) and of $\bar{p}_T$ for constant $\bar{p}_L$ (right hand side). The points shown in Figs. 13-18 are not values directly measured, but are the cross-sections that have been derived by interpolating to the desired $\bar{p}_L$, $\bar{p}_T$ values from the results shown in Figs. 3-8. Fig. 19 gives a recapitulation of the previous six figures on a smaller scale, for ease of an inter-comparison.

From these figures the following conclusions can be drawn.

(i) The proton spectra show a very little longitudinal momentum dependence, a fact noted before by Anderson et al[5]. All other spectra show a strong dependence on both $\bar{p}_L$ and $\bar{p}_T$. The π^+ spectra show in addition some structure referred to above already.

(ii) The curves showing either the $\bar{p}_L$ or the $\bar{p}_T$ dependence for a particular particle, are very similar in shape, at least for $\bar{p}_L \leq 2$ GeV/c. Therefore, the $\bar{p}_L$ and $\bar{p}_T$ dependence of the differential cross-section can be approximately factorized[16]

$$X = f(\bar{p}_L) \cdot g(\bar{p}_T) \cdot$$

The transverse momentum dependence of the protons (Fig. 18) shows clearly that this factorization is only an approximation, since the $\bar{p}_T$ dependence is obviously $\bar{p}_L$ dependent.

(iii) The functional forms of $f(\bar{p}_L)$ and $g(\bar{p}_T)$ are not simple.

The results of this experiment, with its emphasis on measurements at large values of $\bar{p}_L$ and small values at $\bar{p}_T$, are not sufficient to establish the functions f and g. However, with the exception of

the $\bar{p}_L$ dependence of the protons, one might say that both f $(\bar{p}_L)$ and g $(\bar{p}_T)$ look rather exponential, with f $(\bar{p}_L)$ showing in addition a precipitous drop when $\bar{p}_L$ is nearing the kinematic limit and g $(\bar{p}_T)$ indicating some flattening off for small arguments. If this latter fact is indeed true than the derivative $dX/d\bar{p}_T$ would not show a singularity at $\bar{p}_T = 0$.

The $\bar{p}_L$ and $\bar{p}_T$ dependence also shows gaussian characteristics over several decades (not shown). However, the cross sections for small argument of $\bar{p}_T$ deviate from a gaussian and show a strong peaking when plotted against $\bar{p}_T^2$. This phenomenon is also clearly visible in the published $\pi^{\pm}$ and p spectra at 12 GeV/c incident momentum[6d,6e].

The history of models purporting to describe the particle production process is a long one. Recent contributions have been made by Hagedorn and Ranft[17], who base themselves on a thermodynamic model, by Wayland[18], using a two-temperature thermodynamic model and by Caneshi and Pignotti[19], who start from a multi-Regge model. The functions they use are complex, with many free parameters and the predictive power is not clear. Fits to the previously existing data were, however, often ite acceptable. The thermodynamic model has been adjusted by Ranft[17b] to fit also the data of the present experiment.

4. RESULTS ON THE NUCLEAR TARGETS

Table 3 collects the laboratory production cross-sections per nucleus, for a Be, Al, Cu, Pb and B_4C target. The latter compound has been included as it has been used as target material in neutrino experiments. These cross-sections might be expected to be about $A^{2/3}$ times the cross-section on a proton target, because the total absorption cross-sections on nuclei follow approximately this behaviour. Here A is the atomic number of the nucleus. Calling the laboratory differential cross-section per nucleus

$$Q(A) \equiv \frac{d^2\sigma}{d\Omega dp}$$

we will consider the ratio

$$R = \frac{Q(A)}{A^{2/3}\ Q(1)}$$

Deviations of R from 1 will show deviations from this simple proportionality to the nuclear surface area, for instance due to secondary interactions inside the nucleus or to coherent effects.

It turns out that i) R increases monotonically in going from 12 to 70 mrad. ii) R is the same for π^-, K^- and $\bar{p}$ particle production, within the accuracy of the experiment. K^+ and p also give values of R, that are rather similar to the ratio for the three negative particles. The π^+ data show a somewhat a different behaviour.

A small sample of the R values is shown in Fig. 20. In view of the above considerations the results are given only for π^+ and π^- production, for the 2 extreme angles, $12\frac{1}{2}$ and 70 mrad. The variable on the abscissa is the secondary momentum.

From the graphs one can conclude the following.

(i) The ratio R shows a systematic deviation from 1 as a function of A. For the lighter nuclei $R < 1$, for the heavier ones $R > 1$. This shows that the mass dependence of the cross-section is not exactly proportional to $A^{2/3}$.

(ii) R increases with angle. This widening of the angular distribution might be the result of secondary and higher order reactions inside the nucleus.

(iii) R shows a rather weak momentum dependence except in the case of π^- production near the kinematic limit, where a rather violent increase can be noticed. This is due to the fact that π^- mesons can be produced with a higher maximum momentum on a neutron target than on a proton target because the two reactions responsible for the production of the π^- with the highest momentum are $p + n \rightarrow \pi^- + (p + p)$ and $p + p \rightarrow \pi^- + (p + p + \pi^+)$, respectively.

ACKNOWLEDGEMENTS

We are grateful for the excellent support, which enabled us to perform this experiment. R. Donnet, M. Ferrat and C.A. Ståhlbrandt provided invaluable technical assistance. J. Geibel, G. Matthiae and G. Petrucci gave important contributions to the design of the spectrometer. I. Jarstorff carried out the radioactivity measurements of the aluminium foils. The septum magnet was designed by G. Petrucci. The helium-cooled liquid hydrogen target was built by G. Brand and L. Mazzone. The proton synchrotron Division ensured reliable operation of the machine and the extracted beam.

TABLE 1

LABORATORY CROSS SECTIONS (BARNS/SR.GEV/C) AND THEIR PERCENTAGE ERROR FOR PARTICLE PRODUCTION IN PROTON-PROTON INTERACTIONS AT 19.20 GEV/C AS FUNCTION OF LABORATORY ANGLE (MRAD) AND SECONDARY MOMENTUM (GEV/C).
E+N STANDS FOR A MULTIPLYING FACTOR OF +N POWERS OF 10.
ERROR = -1 MEANS CORRESPONDING MEASUREMENT RESULTED IN ZERO COUNTS.
NUMBER QUOTED IS THE ONE STANDARD DEVIATION UPPER LIMIT (1 COUNT)

T	ANG	MOM	PI MINUS		PI PLUS		KA MINUS		KA PLUS		ANTI P		PROTON	
H	12.5	4.50	5.45E-2	3	1.22E-1	3	1.81E-3	4	6.11E-3	3	2.49E-4	3	3.36E-2	10
H	20.0	4.50	5.10E-2	3	1.15E-1	3	1.60E-3	4	5.74E-3	3	2.25E-4	3	3.54E-2	10
H	30.0	4.50	5.28E-2	3	1.10E-1	3	1.71E-3	4	5.52E-3	3	2.40E-4	3	3.17E-2	10
H	40.0	4.50	4.51E-2	3	9.71E-2	3	1.48E-3	3	5.11E-3	3	2.18E-4	3	2.95E-2	10
H	50.0	4.50	4.10E-2	3	7.82E-2	3	1.44E-3	4	4.80E-3	3	2.04E-4	3	2.94E-2	10
H	60.0	4.50	3.44E-2	3	6.51E-2	3	1.37E-3	4	4.52E-3	3	1.92E-4	3	2.55E-2	10
H	70.0	4.50	2.80E-2	3	5.09E-2	3	1.18E-3	4	4.10E-3	3	1.66E-4	4	2.61E-2	10
H	12.5	6.00	4.07E-2	3	1.24E-1	3	1.25E-3	3	5.04E-3	3	1.58E-4	3	7.13E-2	7
H	20.0	6.00	3.80E-2	3	1.12E-1	3	1.20E-3	3	5.03E-3	3	1.49E-4	3	6.57E-2	7
H	30.0	6.00	3.02E-2	3	8.64E-2	3	1.02E-3	3	4.86E-3	3	1.36E-4	3	6.06E-2	7
H	40.0	6.00	2.43E-2	5	6.37E-2	3	9.02E-4	3	4.58E-3	3	1.24E-4	3	5.45E-2	7
H	50.0	6.00	2.06E-2	3	4.67E-2	3	8.00E-4	3	4.04E-3	3	1.07E-4	3	4.80E-2	7
H	60.0	6.00	1.64E-2	3	3.60E-2	3	6.36E-4	3	3.58E-3	3	9.21E-5	3	4.21E-2	7
H	70.0	6.00	1.31E-2	3	2.80E-2	3	5.02E-4	3	3.10E-3	3	7.51E-5	3	3.63E-2	7
H	12.5	8.00	2.18E-2	3	5.73E-2	3	6.68E-4	3	3.97E-3	3	5.56E-5	3	1.18E-1	5
H	20.0	8.00	1.93E-2	3	5.02E-2	3	5.93E-4	3	3.88E-3	3	5.08E-5	3	1.08E-1	5
H	30.0	8.00	1.50E-2	3	3.79E-2	3	4.97E-4	3	3.43E-3	3	4.85E-5	3	9.01E-2	5
H	40.0	8.00	1.17E-2	3	2.80E-2	3	3.58E-4	3	2.91E-3	3	3.43E-5	3	7.57E-2	5
H	50.0	8.00	8.74E-3	3	2.02E-2	5	2.75E-4	3	2.41E-3	5	2.82E-5	3	6.13E-2	5
H	60.0	8.00	6.38E-3	3	1.44E-2	3	1.92E-4	3	1.86E-3	3	2.28E-5	3	4.76E-2	5
H	70.0	8.00	4.60E-3	3	1.06E-2	3	1.42E-4	3	1.37E-3	3	1.54E-5	3	3.59E-2	5
H	12.5	10.00	1.21E-2	3	3.69E-2	3	2.24E-4	3	2.90E-3	3	1.42E-5	4	2.06E-1	3
H	20.0	10.00	1.02E-2	3	3.06E-2	3	1.97E-4	3	2.64E-3	3	1.17E-5	3	1.72E-1	3
H	30.0	10.00	7.82E-3	3	2.13E-2	3	1.59E-4	3	2.19E-3	3	8.99E-6	3	1.25E-1	3
H	35.0	10.00	6.30E-3	3			1.28E-4	3			6.91E-6	4		
H	40.0	10.00	5.75E-3	3	1.37E-2	3	1.15E-4	3	1.66E-3	3	6.59E-6	3	8.92E-2	3
H	50.0	10.00	3.45E-3	3	8.76E-3	3	7.25E-5	3	1.18E-3	3	4.39E-6	3	6.23E-2	3
H	60.0	10.00	2.03E-3	3	5.92E-3	3	4.46E-5	3	7.68E-4	3	2.85E-6	4	4.20E-2	3
H	70.0	10.00	1.35E-3	3	4.04E-3	3	2.85E-5	3	4.95E-4	3	1.96E-6	4	2.81E-2	3
H	12.5	11.00	7.84E-3	3	2.66E-2	3	1.37E-4	3	2.30E-3	3	5.03E-6	3	2.63E-1	3
H	20.0	11.00	6.99E-3	3	2.06E-2	3	1.21E-4	3	1.98E-3	3	4.44E-6	4	2.01E-1	3
H	30.0	11.00	5.63E-3	3	1.39E-2	3	8.61E-5	3	1.55E-3	3	3.12E-6	4	1.33E-1	3
H	35.0	11.00	4.49E-3	3			6.35E-5	5			2.35E-6	6		
H	40.0	11.00	3.58E-3	3	8.57E-3	3	5.36E-5	3	1.11E-3	3	2.09E-6	4	8.62E-2	3
H	50.0	11.00	1.74E-3	3	5.10E-3	5	2.90E-5	3	7.10E-4	5	1.25E-6	4	5.30E-2	5
H	60.0	11.00	1.05E-3	3	3.36E-3	5	1.63E-5	3	4.34E-4	5	7.66E-7	5	3.41E-2	5
H	70.0	11.00	6.09E-4	3	2.11E-3	3	9.37E-6	3	2.66E-4	3	4.19E-7	5	2.22E-2	3
H	12.5	12.00	4.61E-3	3	1.72E-2	3	6.26E-5	3	1.89E-3	3	1.43E-6	4	3.12E-1	3
H	20.0	12.00	4.63E-3	3	1.35E-2	3	5.21E-5	3	1.50E-3	3	1.24E-6	4	2.27E-1	3
H	30.0	12.00	3.29E-3	3	8.17E-3	3	3.28E-5	3	1.07E-3	3	8.37E-7	5	1.36E-1	3
H	35.0	12.00	2.12E-3	3			2.15E-5	3			5.13E-7	10		
H	40.0	12.00	1.56E-3	3	4.80E-3	3	1.70E-5	3	7.05E-4	3	4.23E-7	6	8.08E-2	3
H	50.0	12.00	8.07E-4	3	2.83E-3	3	8.70E-6	3	4.05E-4	3	2.34E-7	7	4.68E-2	3
H	60.0	12.00	4.62E-4	3	1.64E-3	3	4.70E-6	4	2.30E-4	3	1.45E-7	9	2.78E-2	3
H	70.0	12.00	2.41E-4	3	8.68E-4	3	2.50E-6	4	1.20E-4	3	6.38E-8	11	1.58E-2	3
H	12.5	13.00	2.19E-3	3	1.28E-2	3	1.60E-5	3	1.42E-3	3	2.63E-7	6	3.41E-1	3
H	20.0	13.00	2.07E-3	3	8.17E-3	3	1.39E-5	3	1.03E-3	3	1.97E-7	8	2.42E-1	3
H	30.0	13.00	1.16E-3	3	4.43E-3	3	8.29E-6	3	6.82E-4	3	1.03E-7	9	1.33E-1	3
H	35.0	13.00	7.99E-4	3			5.52E-6	3			7.33E-8	9		
H	40.0	13.00	5.94E-4	3	2.48E-3	3	4.02E-6	4	4.17E-4	3	6.41E-8	11	7.33E-2	3
H	50.0	13.00	3.05E-4	3	1.19E-3	3	1.95E-6	5	1.98E-4	3	3.08E-8	19	3.39E-2	3
H	60.0	13.00	1.72E-4	3	7.20E-4	3	1.17E-6	5	1.10E-4	3	1.03E-8	34	2.13E-2	3
H	70.0	13.00	7.88E-5	3	3.53E-4	3	5.58E-7	8	5.26E-5	3	6.95E-9	41	1.10E-2	3
H	12.5	14.00	1.14E-3	3	7.12E-3	5	2.98E-6	3	8.53E-4	5	2.06E-8	16	3.85E-1	5
H	20.0	14.00	6.99E-4	3	4.19E-3	3	2.18E-6	4	6.36E-4	3	1.28E-8	28	2.58E-1	3
H	30.0	14.00	3.85E-4	3	1.96E-3	3	1.18E-6	5	3.91E-4	3	2.96E-9	58	1.27E-1	3
H	35.0	14.00	2.66E-4	3			8.32E-7	7			5.09E-9	49		
H	40.0	14.00	1.97E-4	3	1.06E-3	3	5.93E-7	6	2.19E-4	3	2.44E-9	58	6.38E-2	3
H	50.0	14.00	9.88E-5	3	5.58E-4	5	2.52E-7	9	1.05E-4	5	2.48E-9	58	3.04E-2	5
H	60.0	14.00	4.77E-5	3	2.95E-4	3	1.28E-7	15	4.72E-5	3	2.36E-9	71	1.56E-2	3
H	70.0	14.00	2.09E-5	3	1.26E-4	3			2.01E-5	3			7.37E-3	3
H	12.5	15.00			2.55E-3	5			5.38E-4	5			4.43E-1	5
H	20.0	15.00			1.62E-3	3			3.60E-4	3			2.70E-1	3
H	30.0	15.00			8.48E-4	3			2.01E-4	3			1.20E-1	3
H	35.0	15.00	9.86E-5	3			8.40E-8	33			4.50E-9	-1		
H	40.0	15.00			4.46E-4	3			9.98E-5	3			5.43E-2	3
H	50.0	15.00			2.32E-4	3			4.22E-5	3			2.42E-2	3
H	60.0	15.00			1.03E-4	3			1.67E-5	3			1.09E-2	3
H	70.0	15.00			3.76E-5	3			5.86E-6	3			4.62E-3	3

T	ANG	MOM	PI MINUS	PI PLUS	KA MINUS	KA PLUS	ANTI P	PROTON
H	12.5	16.00		1.59E-3 5		2.59E-4 10		5.21E-1 5
H	20.0	16.00		8.09E-4 3		1.46E-4 3		2.80E-1 3
H	30.0	16.00		3.11E-4 3		6.84E-5 3		1.16E-1 3
H	35.0	16.00	2.68E-5 3					
H	40.0	16.00		1.52E-4 3		2.94E-5 3		4.82E-2 3
H	50.0	16.00		6.88E-5 5		1.00E-5 5		1.85E-2 5
H	60.0	16.00		2.33E-5 5		3.16E-6 6		7.36E-3 5
H	70.0	16.00		6.81E-6 3		9.18E-7 6		2.74E-3 3
H	12.5	13.50		9.16E-3 3	6.42E-6 4	1.02E-3 5	5.00E-8 18	3.49E-1 3
H	12.5	13.80		7.94E-3 3	3.90E-6 4	9.17E-4 5	2.91E-8 23	3.66E-1 3
H	12.5	14.10		6.37E-3 3	2.03E-6 4	7.88E-4 5	1.02E-8 29	3.78E-1 3
H	12.5	14.40	7.21E-4 3	4.69E-3 3	1.16E-6 4	6.90E-4 5	5.70E-9 25	3.94E-1 3
H	12.5	14.70		3.27E-3 3	6.25E-7 6	5.91E-4 5	3.80E-9 -1	4.09E-1 3
H	12.5	14.90	3.94E-4 3					
H	12.5	15.00	3.31E-4 3	2.36E-3 3	2.44E-7 9	4.95E-4 5		4.20E-1 3
H	12.5	15.30	2.43E-4 3	1.86E-3 3	1.01E-7 13	4.02E-4 5		4.36E-1 3
H	12.5	15.60	1.83E-4 3	1.63E-3 3	3.45E-8 21	3.15E-4 5		4.47E-1 3
H	12.5	15.90	1.29E-4 3	1.52E-3 3	2.27E-8 41	2.44E-4 5		4.62E-1 3
H	12.5	16.20	8.80E-5 3	1.19E-3 3		1.74E-4 5		4.75E-1 3
H	12.5	16.50	5.90E-5 3	8.18E-4 3		1.19E-4 5		4.89E-1 3
H	12.5	16.65	4.00E-5 7	6.44E-4 3		8.99E-5 6		5.02E-1 3
H	12.5	16.73	3.51E-5 7	5.94E-4 3		7.00E-5 6		4.99E-1 3
H	12.5	16.80	3.11E-5 7	5.49E-4 3		6.50E-5 6		4.99E-1 3
H	12.5	16.87	2.55E-5 7	5.07E-4 3		5.19E-5 7		4.96E-1 3
H	12.5	16.93	2.31E-5 8	4.72E-4 3		4.83E-5 7		5.11E-1 3
H	12.5	16.95	2.34E-5 8	4.53E-4 3		3.89E-5 6		5.19E-1 3
H	12.5	17.03	1.89E-5 8	4.09E-4 3		3.44E-5 7		5.16E-1 3
H	12.5	17.10	1.45E-5 8	3.52E-4 3		2.37E-5 7		5.14E-1 3
H	12.5	17.17	9.00E-6 10	3.04E-4 3		1.95E-5 8		5.09E-1 3
H	12.5	17.23	5.60E-6 15	2.90E-4 3		1.54E-5 9		5.25E-1 3
H	12.5	17.25	5.19E-6 15	2.53E-4 3		1.10E-5 8		5.28E-1 3
H	12.5	17.32	1.51E-6 50	2.17E-4 3		6.25E-6 9		5.24E-1 3
H	12.5	17.40	4.00E-7 -1	1.71E-4 3		4.29E-6 11		5.17E-1 3
H	12.5	17.47	3.50E-7 -1	1.44E-4 3		1.68E-6 16		5.14E-1 3
H	12.5	17.54		1.32E-4 3		8.15E-7 23		5.30E-1 3
H	12.5	17.54		1.17E-4 5		4.47E-7 27		5.28E-1 3
H	12.5	17.62		8.98E-5 5		1.22E-7 50		5.29E-1 3
H	12.5	17.70		7.04E-5 5		6.33E-8 71		5.39E-1 3
H	12.5	17.77		7.94E-5 5		3.24E-8 90		5.55E-1 3
H	12.5	17.84		5.08E-5 6		7.28E-8 71		5.94E-1 3
H	12.5	17.84		2.50E-5 6		2.50E-8 -1		4.59E-1 3
H	12.5	17.92		2.80E-6 20		2.50E-8 -1		6.50E-1 3
H	12.5	18.00		1.00E-6 90		2.50E-8 -1		7.61E-1 3
H	12.5	18.07		1.00E-6 90		2.50E-8 -1		8.77E-1 3
H	12.5	18.14		1.00E-6 90		2.50E-8 -1		9.39E-1 3
H	12.5	18.14		1.40E-7 90				9.55E-1 3
H	12.5	18.22		7.30E-8 90				9.16E-1 3
H	12.5	18.30		2.50E-8 -1				8.98E-1 3
H	12.5	18.37		1.00E-7 90				9.82E-1 3
H	12.5	18.44		8.70E-8 90				1.14E-0 3
H	12.5	18.60						1.20E-0 5
H	12.5	18.90						8.79E-1 5
H	12.5	19.20						1.30E+1 5
H	20.0	13.50		6.15E-3 3		8.29E-4 5		2.39E-1 3
H	20.0	13.80		5.06E-3 3		7.08E-4 5		2.42E-1 3
H	20.0	14.10		3.92E-3 3		6.07E-4 5		2.45E-1 3
H	20.0	14.40		2.86E-3 3		5.30E-4 5		2.47E-1 3
H	20.0	14.70		2.10E-3 3		4.47E-4 5		2.49E-1 3
H	20.0	15.00		1.60E-3 3		3.68E-4 5		2.50E-1 3
H	20.0	15.30		1.26E-3 3		2.92E-4 5		2.50E-1 3
H	20.0	15.60		1.04E-3 3		2.24E-4 5		2.50E-1 3
H	20.0	15.90		8.53E-4 3		1.68E-4 5		2.50E-1 3
H	20.0	16.20		6.22E-4 3		1.17E-4 5		2.52E-1 3
H	20.0	16.50		4.15E-4 3		7.27E-5 5		2.55E-1 3
H	20.0	16.80		2.74E-4 3		3.88E-5 5		2.63E-1 3
H	20.0	17.10		1.61E-4 3		1.37E-5 5		2.72E-1 3
H	20.0	17.40		8.42E-5 3		1.95E-6 7		2.82E-1 3
H	20.0	17.70		3.47E-5 3		2.75E-8 45		3.04E-1 3
H	20.0	18.00		2.35E-6 10		9.00E-9 -1		4.44E-1 3
H	20.0	18.30		2.50E-7 90		1.30E-8 -1		4.69E-1 3

T	ANG	MOM	PI MINUS	PI PLUS	KA MINUS	KA PLUS	ANTI P	PROTON
H	30.0	13.50		3.13E-3 3		5.35E-4 5		1.25E-1 3
H	30.0	13.80		2.43E-3 3		4.54E-4 5		1.23E-1 3
H	30.0	14.10		1.83E-3 3		3.68E-4 5		1.20E-1 3
H	30.0	14.40		1.37E-3 3		3.11E-4 5		1.18E-1 3
H	30.0	14.70		1.06E-3 3		2.46E-4 5		1.15E-1 3
H	30.0	15.00		8.26E-4 3		2.01E-4 5		1.12E-1 3
H	30.0	15.30		6.32E-4 3		1.55E-4 5		1.10E-1 3
H	30.0	15.60		4.75E-4 3		1.13E-4 5		1.07E-1 3
H	30.0	15.90		3.48E-4 3		8.30E-5 5		1.06E-1 3
H	30.0	16.20		2.39E-4 3		5.42E-5 5		1.05E-1 3
H	30.0	16.50		1.58E-4 3		3.21E-5 5		1.05E-1 3
H	30.0	16.80		9.75E-5 3		1.43E-5 6		1.07E-1 3
H	30.0	17.10		5.50E-5 3		4.55E-6 6		1.09E-1 3
H	30.0	17.40		2.50E-5 3		4.60E-7 20		1.08E-1 3
H	30.0	17.70		7.85E-6 3		7.00E-9 -1		1.23E-1 3
H	30.0	18.00		1.00E-7 90		9.00E-9 -1		1.65E-1 3
H	40.0	16.52						4.53E-2 3
H	40.0	16.82						4.53E-2 3
H	40.0	17.08						4.34E-2 3
H	40.0	17.38						4.16E-2 3
H	40.0	17.68						5.71E-2 3
H	40.0	17.82						7.18E-2 3
H	40.0	17.98						5.41E-2 3
H	40.0	18.12						5.94E-2 3
H	40.0	18.28						4.52E-2 3
H	40.0	18.50						3.13E-2 3
H	40.0	18.66						2.08E-2 3
H	40.0	18.73						3.50E-2 3
H	40.0	18.76						6.88E-2 3
H	40.0	18.78						1.26E-1 3
H	50.0	16.42						1.72E-2 3
H	50.0	16.72						1.65E-2 3
H	50.0	17.02						1.54E-2 3
H	50.0	17.42						1.43E-2 3
H	50.0	17.65						2.09E-2 3
H	50.0	17.80						1.71E-2 3
H	50.0	17.96						1.91E-2 3
H	50.0	18.18						1.37E-2 3
H	50.0	18.33						8.93E-3 3
H	50.0	18.48						5.14E-3 3
H	50.0	18.53						3.30E-3 3
H	50.0	18.61						1.14E-2 3
H	60.0	16.48						6.36E-3 3
H	60.0	16.88						5.41E-3 3
H	60.0	17.18						4.69E-3 3
H	60.0	17.48						5.55E-3 3
H	60.0	17.66						4.45E-3 3
H	60.0	17.78						4.79E-3 3
H	60.0	18.00						3.13E-3 3
H	60.0	18.15						1.82E-3 3
H	60.0	18.28						1.02E-3 3
H	60.0	18.37						4.75E-4 3
H	60.0	18.45						2.70E-3 3
H	70.0	16.53						1.43E-3 3
H	70.0	16.87						1.16E-3 3
H	70.0	17.13						1.03E-3 3
H	70.0	17.28						1.06E-3 3
H	70.0	17.42						7.84E-4 3
H	70.0	17.58						7.52E-4 3
H	70.0	17.72						5.09E-4 3
H	70.0	17.80						3.70E-4 3
H	70.0	17.96						2.52E-4 4
H	70.0	18.11						1.60E-4 3
H	70.0	18.15						3.13E-4 3
H	70.0	18.19						1.10E-3 3

Table 2

Maximum attainable momentum of a particle, produced in proton-proton collisions at 19.20 GeV/c incident momentum, at a laboratory production angle of 12.5 mrad

Secondary Particle	Reaction	Maximum momentum of secondary particle (GeV/c)
π^+	$p + p \rightarrow \pi^+ + D$	17.82
π^-	$p + p \rightarrow \pi^- + (p + p + \pi^+)$	17.55
K^+	$p + p \rightarrow K^+ + (p + \Lambda)$	17.44
K^-	$p + p \rightarrow K^- + (p + p + K^+)$	16.70
p	$p + p \rightarrow p + p$	19.17
$\bar{p}$	$p + p \rightarrow \bar{p} + (p + p + p)$	15.39

TABLE 3

LABORATORY CROSS SECTIONS (BARNS/SR.GEV/C PER NUCLEUS) AND THEIR PERCENTAGE ERROR FOR PARTICLE PRODUCTION IN PROTON-NUCLEUS INTERACTIONS AT 19.2 GEV/C AS FUNCTION OF LABORATORY ANGLE (MRAD) AND MOMENTUM (GEV/C) FOR VARIOUS TARGETS (T)
E+N STANDS FOR A MULTIPLYING FACTOR OF +N POWERS OF 10.
ERROR = -1 MEANS CORRESPONDING MEASUREMENT RESULTED IN ZERO COUNTS.
NUMBER QUOTED IS THE ONE STANDARD DEVIATION UPPER LIMIT (1 COUNT)
TARGET T=BC IS AN ABBREVIATION FOR THE CHEMICAL COMPOUND BORON CARBIDE (B4C)

T	ANG	MOM	PI MINUS		PI PLUS		KA MINUS		KA PLUS		ANTI P		PROTON	
BE	12.5	6.00	2.16E-1	3	5.37E-1	3	6.52E-3	4	2.59E-2	3	8.51E-4	4	3.84E-1	3
BE	20.0	6.00	2.10E-1	3	4.99E-1	3	7.31E-3	4	2.73E-2	3	8.49E-4	4	3.65E-1	3
BE	30.0	6.00	1.83E-1	3	3.94E-1	3	6.38E-3	4	2.56E-2	3	7.80E-4	4	3.45E-1	3
BE	40.0	6.00	1.55E-1	3	2.97E-1	3	5.40E-3	4	2.35E-2	3	7.68E-4	4	3.03E-1	3
BE	50.0	6.00	1.26E-1	3	2.32E-1	3	4.63E-3	4	2.15E-2	3	6.96E-4	4	2.71E-1	3
BE	60.0	6.00	1.04E-1	3	1.82E-1	3	4.13E-3	5	1.99E-2	3	5.88E-4	5	2.29E-1	3
BE	70.0	6.00	8.33E-2	3	1.43E-1	3	3.60E-3	5	1.73E-2	3	4.87E-4	5	1.98E-1	3
BE	12.5	8.00	1.17E-1	3	2.56E-1	3	3.67E-3	3	1.92E-2	3	2.92E-4	4	5.41E-1	3
BE	20.0	8.00	1.04E-1	3	2.24E-1	3	3.19E-3	3	1.91E-2	3	2.99E-4	4	4.98E-1	3
BE	30.0	8.00	8.38E-2	3	1.80E-1	3	2.63E-3	4	1.71E-2	3	2.53E-4	4	4.31E-1	3
BE	40.0	8.00	6.67E-2	3	1.34E-1	3	2.04E-3	4	1.48E-2	3	2.16E-4	4	3.69E-1	3
BE	50.0	8.00	5.24E-2	3	9.77E-2	3	1.68E-3	4	1.25E-2	3	1.82E-4	5	2.98E-1	3
BE	60.0	8.00	4.06E-2	3	6.98E-2	3	1.24E-3	4	9.62E-3	3	1.47E-4	5	2.36E-1	3
BE	70.0	8.00	2.93E-2	3	5.23E-2	3	8.70E-4	5	7.44E-3	3	1.05E-4	6	1.81E-1	3
BE	12.5	10.00	6.27E-2	3	1.67E-1	3	1.17E-3	3	1.34E-2	3	7.34E-5	4	8.97E-1	3
BE	20.0	10.00	5.60E-2	3	1.44E-1	3	1.05E-3	4	1.30E-2	3	6.53E-5	8	8.46E-1	3
BE	30.0	10.00	4.22E-2	3	9.47E-2	3	8.61E-4	3	1.02E-2	3	5.71E-5	5	5.54E-1	3
BE	40.0	10.00	3.10E-2	3	6.45E-2	3	6.22E-4	4	8.35E-3	3	3.67E-5	6	4.24E-1	3
BE	50.0	10.00	1.97E-2	3	4.20E-2	3	3.89E-4	4	6.18E-3	3	3.02E-5	6	3.01E-1	3
BE	60.0	10.00	1.25E-2	3	2.86E-2	3	2.59E-4	4	4.30E-3	3	1.62E-5	8	2.09E-1	3
BE	70.0	10.00	8.40E-3	3	1.92E-2	3	1.63E-4	5	2.85E-3	3	1.43E-5	8	1.44E-1	3
BE	12.5	12.00	2.13E-2	3	7.17E-2	3	2.70E-4	4	8.38E-3	3	8.22E-6	10	1.31E-0	3
BE	20.0	12.00	2.03E-2	3	6.61E-2	3	2.24E-4	3	7.71E-3	3	5.49E-6	5	1.10E-0	3
BE	30.0	12.00	1.41E-2	3	3.89E-2	3	1.49E-4	4	5.59E-3	3	4.71E-6	10	6.37E-1	3
BE	40.0	12.00	7.93E-3	3	2.28E-2	3	8.84E-5	5	3.79E-3	3	3.16E-6	13	3.94E-1	3
BE	50.0	12.00	4.30E-3	3	1.40E-2	3	4.40E-5	6	2.38E-3	3	1.77E-6	17	2.39E-1	3
BE	60.0	12.00	2.42E-3	3	8.13E-3	3	2.57E-5	8	1.41E-3	3	5.31E-7	29	1.44E-1	3
BE	70.0	12.00	1.45E-3	4	4.65E-3	3			7.91E-4	4			8.64E-2	3
BE	12.5	14.00	5.07E-3	3	2.54E-2	3	1.44E-5	9	3.67E-3	3	1.27E-7	75	1.71E-0	3
BE	20.0	14.00	3.63E-3	3	1.67E-2	3	1.24E-5	9	2.93E-3	3			1.15E-0	3
BE	30.0	14.00	1.95E-3	3	8.96E-3	3	4.88E-6	14	2.05E-3	3			5.99E-1	3
BE	40.0	14.00	1.08E-3	3	4.91E-3	3	2.17E-6	18	1.20E-3	4			3.12E-1	3
BE	50.0	14.00	5.78E-4	3	2.77E-3	3	3.01E-7	26	6.32E-4	4			1.61E-1	3
BE	60.0	14.00	2.96E-4	3	1.45E-3	3	1.06E-6	30	3.06E-4	4			8.50E-2	3
BE	70.0	14.00			6.48E-4	3			1.21E-4	6			4.14E-2	3
BE	12.5	16.00			4.75E-3	3			9.44E-4	5			2.11E-0	3
BE	20.0	16.00			2.97E-3	3			6.40E-4	4			1.17E-0	3
BE	30.0	16.00			1.34E-3	3			3.55E-4	4			5.25E-1	3
BE	40.0	16.00			6.47E-4	3			1.86E-4	5			2.32E-1	3
BE	50.0	16.00			3.07E-4	3			6.77E-5	6			9.92E-2	3
BE	60.0	16.00			1.18E-4	4			2.56E-5	10			4.19E-2	3
BE	70.0	16.00			3.74E-5	6			6.92E-6	18			1.57E-2	3
BE	12.5	13.50			3.62E-2	3			4.94E-3	4			1.61E-0	3
BE	12.5	13.80	6.30E-3	3	3.10E-2	3	2.89E-5	10	4.17E-3	5			1.68E-0	3
BE	12.5	14.10	5.05E-3	3	2.43E-2	3	8.87E-6	15	3.71E-3	5			1.74E-0	3
BE	12.5	14.40	3.72E-3	3	1.71E-2	3	1.01E-5	15	3.08E-3	6			1.80E-0	3
BE	12.5	14.70	2.76E-3	3	1.16E-2	3	3.60E-6	22	2.55E-3	6			1.84E-0	3
BE	12.5	15.00	1.99E-3	3	9.15E-3	3	3.47E-6	23	1.87E-3	7			1.88E-0	3
BE	12.5	15.30	1.48E-3	4	7.41E-3	4			1.81E-3	7			1.93E-0	3
BE	12.5	15.60	1.09E-3	4	6.16E-3	4			1.27E-3	8			1.95E-0	3
BE	12.5	15.90	8.37E-4	5	4.99E-3	4			1.07E-3	10			2.01E-0	3
BE	12.5	16.20	6.06E-4	5	3.80E-3	3			6.42E-4	8			2.06E-0	3
BE	12.5	16.50	4.21E-4	5	2.52E-3	4			5.06E-4	7			2.09E-0	3
BE	12.5	16.80	3.07E-4	5	1.61E-3	4			2.86E-4	8			2.12E-0	3
BE	12.5	17.10	2.08E-4	6	9.87E-4	4			9.14E-5	28			2.16E-0	3
BE	12.5	17.17			8.00E-4	4			5.84E-5	35			2.13E-0	3
BE	12.5	17.23			8.02E-4	4			4.04E-5	41			2.19E-0	3
BE	12.5	17.25			6.97E-4	4			3.33E-5	53			2.21E-0	3
BE	12.5	17.32			6.14E-4	5			2.87E-5	32			2.21E-0	3
BE	12.5	17.40	9.82E-5	7	5.08E-4	5			3.38E-5	30			2.21E-0	3
BE	12.5	17.47	8.30E-5	8	4.18E-4	5			2.13E-5	38			2.20E-0	3
BE	12.5	17.54	7.23E-5	8	3.08E-4	5			2.10E-6	90			2.29E-0	3
BE	12.5	17.62	4.80E-5	10	2.44E-4	6			1.61E-6	90			2.32E-0	3
BE	12.5	17.70	3.77E-5	11	1.35E-4	8			1.72E-6	90			2.41E-0	3
BE	12.5	17.77	2.18E-5	15	1.16E-4	9			1.71E-6	90			2.50E-0	3
BE	12.5	17.84	1.30E-5	18	8.22E-5	9							2.69E-0	3
BE	12.5	17.92	8.29E-6	22	3.97E-5	14							2.85E-0	3
BE	12.5	18.00	8.54E-7	58	9.08E-6	25							3.09E-0	3
BE	12.5	18.07	8.95E-7	71	6.32E-6	38							3.26E-0	3
BE	12.5	18.14	4.50E-7	-1	3.01E-6	50							3.47E-0	3

T	ANG	MOM	PI MINUS		PI PLUS		KA MINUS		KA PLUS		ANTI P		PROTON	
AL	12.5	6.00	4.30E-1	3	9.92E-1	3	1.43E-2	4	5.81E-2	3	1.73E-3	4	8.32E-1	3
AL	20.0	6.00	4.15E-1	3	9.13E-1	3	1.30E-2	4	5.86E-2	3	1.78E-3	4	7.86E-1	3
AL	30.0	6.00	3.63E-1	3	7.53E-1	3	1.33E-2	4	5.64E-2	3	1.64E-3	4	7.45E-1	3
AL	40.0	6.00	3.10E-1	3	5.86E-1	3	1.17E-2	3	5.42E-2	3	1.46E-3	3	6.56E-1	3
AL	50.0	6.00	2.56E-1	3	4.61E-1	3	1.03E-2	5	4.76E-2	3	1.29E-3	5	5.88E-1	3
AL	60.0	6.00	2.12E-1	3	3.72E-1	3	8.53E-3	5	4.37E-2	3	1.20E-3	5	5.08E-1	3
AL	70.0	6.00	1.68E-1	3	2.88E-1	3	7.51E-3	5	3.80E-2	3	1.02E-3	5	4.35E-1	3
AL	12.5	8.00	2.23E-1	3	4.75E-1	3	7.26E-3	3	4.06E-2	3	5.23E-4	4	1.07E-0	3
AL	20.0	8.00	1.98E-1	3	4.25E-1	3	5.80E-3	4	3.76E-2	3	5.62E-4	4	9.91E-1	3
AL	30.0	8.00	1.65E-1	3	3.45E-1	3	5.22E-3	4	3.45E-2	3	4.82E-4	5	8.55E-1	3
AL	40.0	8.00	1.07E-1	3	2.61E-1	3	3.85E-3	4	2.98E-2	3	3.98E-4	5	7.32E-1	3
AL	50.0	8.00	1.04E-1	3	1.92E-1	3	3.11E-3	4	2.58E-2	3	3.33E-4	5	5.91E-1	3
AL	60.0	8.00	7.83E-2	3	1.37E-1	3	2.45E-3	5	1.97E-2	3	2.44E-4	6	4.78E-1	3
AL	70.0	8.00	5.95E-2	3	1.03E-1	3	1.86E-3	5	1.59E-2	3	2.12E-4	6	3.70E-1	3
AL	12.5	10.00	1.14E-1	3	3.06E-1	3	2.09E-3	3	2.53E-2	3	1.23E-4	5	1.63E-0	3
AL	20.0	10.00	1.02E-1	3	2.56E-1	3	1.85E-3	4	2.41E-2	3	1.13E-4	7	1.40E-0	3
AL	30.0	10.00	7.59E-2	3	1.73E-1	3	1.53E-3	4	1.93E-2	3	8.38E-5	6	1.01E-0	3
AL	40.0	10.00	5.64E-2	3	1.19E-1	3	1.16E-3	4	1.63E-2	3	6.71E-5	7	7.91E-1	3
AL	50.0	10.00	3.61E-2	3	7.95E-2	3	7.86E-4	4	1.27E-2	3	4.87E-5	8	5.71E-1	3
AL	60.0	10.00	2.41E-2	3	5.49E-2	3	5.06E-4	4	8.76E-3	3	3.49E-5	7	4.03E-1	3
AL	70.0	10.00	1.61E-2	3	3.70E-2	3	3.43E-4	6	6.16E-3	3	2.48E-5	10	2.83E-1	3
AL	12.5	12.00	3.55E-2	3	1.24E-1	3	4.40E-4	4	1.59E-2	3	1.13E-5	11	2.26E-0	3
AL	20.0	12.00	3.33E-2	3	1.20E-1	3	3.84E-4	4	1.48E-2	3	1.08E-5	10	1.97E-0	3
AL	30.0	12.00	2.38E-2	3	6.93E-2	3	2.44E-4	5	1.02E-2	3	5.76E-6	14	1.11E-0	3
AL	40.0	12.00	1.40E-2	3	4.14E-2	3	1.51E-4	6	7.45E-3	3	3.19E-6	19	7.12E-1	3
AL	50.0	12.00	7.95E-3	3	2.58E-2	3	8.97E-5	7	4.80E-3	3	2.72E-6	22	4.42E-1	3
AL	60.0	12.00	4.78E-3	3	1.49E-2	3	5.73E-5	8	2.78E-3	4	1.09E-6	32	2.74E-1	3
AL	70.0	12.00	2.83E-3	3	8.51E-3	3			1.61E-3	4			1.67E-1	3
AL	12.5	14.00	8.27E-3	3	4.22E-2	3	2.86E-5	9	6.66E-3	4	2.10E-7	-1	2.84E-0	3
AL	20.0	14.00	6.00E-3	3	2.87E-2	3	2.16E-5	10	5.60E-3	4			1.94E-0	3
AL	30.0	14.00	3.42E-3	3	1.56E-2	3	1.51E-5	13	3.84E-3	4			1.02E-0	3
AL	40.0	14.00	1.88E-3	3	8.78E-3	3	5.82E-6	18	2.28E-3	4			5.56E-1	3
AL	50.0	14.00	1.06E-3	3	4.97E-3	3	1.90E-6	-1	1.32E-3	4			2.98E-1	3
AL	60.0	14.00	5.45E-4	4	2.69E-3	3	1.65E-6	71	6.72E-4	5			1.60E-1	3
AL	70.0	14.00			1.26E-3	3			3.09E-4	6			8.16E-2	3
AL	12.5	16.00			7.60E-3	3			1.59E-3	5			3.42E-0	3
AL	20.0	16.00			4.87E-3	3			1.19E-3	4			1.92E-0	3
AL	30.0	16.00			2.29E-3	3			6.42E-4	4			8.92E-1	3
AL	40.0	16.00			1.12E-3	3			3.33E-4	4			4.11E-1	3
AL	50.0	16.00			5.39E-4	4			1.31E-4	7			1.86E-1	3
AL	60.0	16.00			2.21E-4	5			4.12E-5	13			8.09E-2	3
AL	70.0	16.00			7.38E-5	7			1.59E-5	20			3.26E-2	3
AL	12.5	13.50			6.14E-2	3			9.45E-3	4			2.70E-0	3
AL	12.5	13.80	1.02E-2	3	5.18E-2	3	4.92E-5	12	7.92E-3	5			2.79E-0	3
AL	12.5	14.10	8.19E-3	3	4.01E-2	3	2.18E-5	16	6.40E-3	5			2.89E-0	3
AL	12.5	14.40	5.96E-3	3	2.95E-2	3	1.95E-5	18	5.40E-3	5			2.98E-0	3
AL	12.5	14.70	4.35E-3	3	2.07E-2	3	1.25E-5	20	4.89E-3	5			3.06E-0	3
AL	12.5	15.00	3.29E-3	3	1.50E-2	3	1.44E-6	40	3.50E-3	6			3.10E-0	3
AL	12.5	15.30	2.40E-3	4	1.26E-2	4			3.33E-3	6			3.17E-0	3
AL	12.5	15.60	1.82E-3	5	1.03E-2	4			2.37E-3	7			3.19E-0	3
AL	12.5	15.90	1.34E-3	5	8.24E-3	4			1.69E-3	9			3.31E-0	3
AL	12.5	16.20	9.16E-4	5	6.29E-3	4			1.38E-3	9			3.36E-0	3
AL	12.5	16.50	5.95E-4	5	4.23E-3	4			8.95E-4	9			3.35E-0	3
AL	12.5	16.80	4.30E-4	6	2.69E-3	4			5.32E-4	11			3.37E-0	3
AL	12.5	17.10	2.84E-4	5	1.66E-3	5			2.37E-4	29			3.41E-0	3
AL	12.5	17.17			1.35E-3	5			2.06E-4	30			3.37E-0	3
AL	12.5	17.23			1.33E-3	5			1.42E-4	42			3.47E-0	3
AL	12.5	17.25			1.31E-3	5			8.47E-5	57			3.47E-0	3
AL	12.5	17.32			1.04E-3	5			1.27E-4	25			3.44E-0	3
AL	12.5	17.40	1.83E-4	7	8.13E-4	6			3.41E-5	50			3.46E-0	3
AL	12.5	17.47	1.34E-4	8	6.28E-4	7			8.46E-6	90			3.44E-0	3
AL	12.5	17.54	9.93E-5	9	5.36E-4	7			4.00E-6	90			3.57E-0	3
AL	12.5	17.62	6.65E-5	11	4.48E-4	7			4.47E-6	90			3.60E-0	3
AL	12.5	17.70	5.21E-5	13	3.23E-4	9			5.00E-6	-1			3.75E-0	3
AL	12.5	17.77	3.51E-5	16	2.24E-4	11							3.87E-0	3
AL	12.5	17.84	2.76E-5	19	1.49E-4	10							4.16E-0	3
AL	12.5	17.92	7.71E-6	35	7.28E-5	17							4.42E-0	3
AL	12.5	18.00	4.14E-6	50	1.77E-5	28							4.79E-0	3
AL	12.5	18.07	1.37E-6	90	1.76E-5	38							5.05E-0	3
AL	12.5	18.14	1.40E-6	-1	1.11E-5	45							5.38E-0	3

T	ANG	MOM	PI MINUS		PI PLUS		KA MINUS		KA PLUS		ANTI P		PROTON	
CU	12.5	6.00	7.20E-1	3	1.56E-0	3	2.26E-2	4	1.03E-1	3	2.57E-3	5	1.39E-0	3
CU	20.0	6.00	6.85E-1	3	1.47E-0	3	2.45E-2	4	1.01E-1	3	2.62E-3	5	1.36E-0	3
CU	30.0	6.00	6.09E-1	3	1.23E-0	3	2.20E-2	5	9.81E-2	3	2.57E-3	5	1.30E-0	3
CU	40.0	6.00	5.25E-1	3	9.61E-1	3	1.81E-2	5	9.70E-2	3	2.18E-3	5	1.14E-0	3
CU	50.0	6.00	4.29E-1	3	7.64E-1	3	1.64E-2	5	8.70E-2	3	1.90E-3	5	1.03E-0	3
CU	60.0	6.00	3.60E-1	3	6.18E-1	3	1.53E-2	4	7.89E-2	3	1.90E-3	4	8.90E-1	3
CU	70.0	6.00	2.79E-1	3	4.87E-1	3	1.14E-2	5	6.75E-2	3	1.71E-3	5	7.76E-1	3
CU	12.5	8.00	3.61E-1	3	7.48E-1	3	1.12E-2	4	6.72E-2	3	7.84E-4	5	1.73E-0	3
CU	20.0	8.00	3.19E-1	3	6.79E-1	3	9.27E-3	4	6.25E-2	3	8.05E-4	5	1.62E-0	3
CU	30.0	8.00	2.71E-1	3	5.56E-1	3	8.51E-3	4	5.94E-2	3	6.62E-4	5	1.40E-0	3
CU	40.0	8.00	2.17E-1	3	4.24E-1	3	6.60E-3	4	5.20E-2	3	5.68E-4	6	1.21E-0	3
CU	50.0	8.00	1.72E-1	3	3.12E-1	3	5.46E-3	4	4.41E-2	3	4.86E-4	6	9.78E-1	3
CU	60.0	8.00	1.32E-1	3	2.26E-1	3	4.16E-3	5	3.53E-2	3	4.23E-4	6	7.97E-1	3
CU	70.0	8.00	9.91E-2	3	1.71E-1	3	3.01E-3	5	2.86E-2	3	3.21E-4	7	6.26E-1	3
CU	12.5	10.00	1.76E-1	3	4.78E-1	3	3.25E-3	4	4.17E-2	3	1.94E-4	5	2.55E-0	3
CU	20.0	10.00	1.57E-1	3	3.97E-1	3	2.82E-3	4	3.98E-2	3	1.53E-4	6	2.21E-0	3
CU	30.0	10.00	1.21E-1	3	2.71E-1	3	2.52E-3	4	3.29E-2	3	1.59E-4	6	1.57E-0	3
CU	40.0	10.00	8.98E-2	3	1.89E-1	3	1.87E-3	4	2.76E-2	3	1.05E-4	7	1.27E-0	3
CU	50.0	10.00	5.89E-2	3	1.28E-1	3	1.31E-3	5	2.11E-2	3	6.46E-5	9	9.30E-1	3
CU	60.0	10.00	3.90E-2	3	8.75E-2	3	8.79E-4	5	1.54E-2	3	5.14E-5	10	6.62E-1	3
CU	70.0	10.00	2.64E-2	3	5.92E-2	3	6.15E-4	7	1.11E-2	3	3.67E-5	14	4.66E-1	3
CU	12.5	12.00	5.57E-2	3	1.92E-1	3	7.27E-4	4	2.50E-2	3	1.85E-5	12	3.49E-0	3
CU	20.0	12.00	5.15E-2	3	1.63E-1	3	6.05E-4	4	2.08E-2	3	1.26E-5	13	2.67E-0	3
CU	30.0	12.00	3.71E-2	3	1.07E-1	3	4.22E-4	5	1.72E-2	3	8.44E-6	14	1.72E-0	3
CU	40.0	12.00	2.17E-2	3	6.46E-2	3	2.56E-4	5	1.21E-2	3	5.54E-6	18	1.11E-0	3
CU	50.0	12.00	1.23E-2	3	4.02E-2	3	1.53E-4	8	7.72E-3	4	4.64E-6	25	6.97E-1	3
CU	60.0	12.00	7.57E-3	3	2.42E-2	3	8.17E-5	10	5.03E-3	4	3.21E-6	29	4.45E-1	3
CU	70.0	12.00	4.46E-3	4	1.38E-2	3			3.07E-3	4			2.72E-1	3
CU	12.5	14.00	1.31E-2	3	6.52E-2	3	4.05E-5	12	1.12E-2	4	3.98E-7	90	4.26E-0	3
CU	20.0	14.00	9.31E-3	3	4.38E-2	3	3.78E-5	11	8.42E-3	4			2.95E-0	3
CU	30.0	14.00	5.48E-3	3	2.42E-2	3	1.87E-5	17	6.07E-3	4			1.58E-0	3
CU	40.0	14.00	3.08E-3	3	1.36E-2	3	1.13E-5	19	3.83E-3	4			8.67E-1	3
CU	50.0	14.00	1.66E-3	3	7.54E-3	3	9.06E-7	33	2.25E-3	4			4.71E-1	3
CU	60.0	14.00	9.45E-4	4	4.34E-3	3	1.80E-6	90	1.14E-3	5			2.59E-1	3
CU	70.0	14.00			2.20E-3	4			5.50E-4	6			1.36E-1	3
CU	12.5	16.00			1.13E-2	3			2.47E-3	5			5.14E-0	3
CU	20.0	16.00			7.37E-3	3			1.81E-3	4			2.89E-0	3
CU	30.0	16.00			3.59E-3	3			1.03E-3	4			1.36E-0	3
CU	40.0	16.00			1.71E-3	3			5.39E-4	6			6.40E-1	3
CU	50.0	16.00			8.27E-4	4			2.16E-4	8			2.95E-1	3
CU	60.0	16.00			3.50E-4	5			9.26E-5	12			1.32E-1	3
CU	70.0	16.00			1.10E-4	8			2.89E-5	21			5.49E-2	3
PB	12.5	6.00	1.18E-0	3	2.55E-0	3	4.35E-2	5	1.76E-1	3	4.37E-3	5	2.37E-0	3
PB	20.0	6.00	1.18E-0	3	2.44E-0	3	4.01E-2	5	1.92E-1	3	4.04E-3	5	2.35E-0	3
PB	30.0	6.00	1.05E-0	3	2.07E-0	3	4.10E-2	5	1.82E-1	4	4.31E-3	5	2.34E-0	3
PB	40.0	6.00	9.04E-1	3	1.59E-0	3	3.55E-2	5	1.66E-1	4	3.82E-3	6	2.01E-0	3
PB	50.0	6.00	7.19E-1	3	1.28E-0	3	2.83E-2	5	1.64E-1	3	3.69E-3	5	1.82E-0	3
PB	60.0	6.00	6.26E-1	3	1.03E-0	3	2.70E-2	5	1.47E-1	3	3.31E-3	5	1.58E-0	3
PB	70.0	6.00	4.72E-1	3	8.26E-1	3	2.10E-2	5	1.30E-1	4	2.41E-3	5	1.39E-0	3
PB	12.5	8.00	5.92E-1	3	1.18E-0	3	1.73E-2	4	1.12E-1	3	1.27E-3	5	2.80E-0	3
PB	20.0	8.00	5.27E-1	3	1.08E-0	3	1.55E-2	4	1.10E-1	3	1.33E-3	5	2.64E-0	3
PB	30.0	8.00	4.63E-1	3	8.91E-1	3	1.23E-2	4	1.01E-1	3	1.13E-3	6	2.33E-0	3
PB	40.0	8.00	3.60E-1	3	6.69E-1	3	1.06E-2	5	8.69E-2	3	8.02E-4	7	2.01E-0	3
PB	50.0	8.00	2.92E-1	3	5.12E-1	3	9.07E-3	5	7.43E-2	3	8.42E-4	7	1.67E-0	3
PB	60.0	8.00	2.29E-1	3	3.73E-1	3	7.60E-3	4	6.17E-2	3	5.95E-4	6	1.35E-0	3
PB	70.0	8.00	1.60E-1	3	2.82E-1	3	5.66E-3	5	4.90E-2	3	5.38E-4	7	1.07E-0	3
PB	12.5	10.00	2.73E-1	3	7.29E-1	3	5.16E-3	4	6.91E-2	3	3.22E-4	6	4.02E-0	3
PB	20.0	10.00	2.41E-1	3	6.12E-1	3	4.96E-3	4	6.95E-2	3	2.58E-4	7	3.52E-0	3
PB	30.0	10.00	1.95E-1	3	4.14E-1	3	4.28E-3	4	5.49E-2	3	2.11E-4	8	2.44E-0	3
PB	40.0	10.00	1.46E-1	3	3.04E-1	3	3.06E-3	5	4.88E-2	3	1.74E-4	9	2.06E-0	3
PB	50.0	10.00	9.81E-2	3	2.07E-1	3	2.13E-3	5	3.61E-2	3	1.01E-4	9	1.52E-0	3
PB	60.0	10.00	6.47E-2	3	1.43E-1	3	1.45E-3	5	2.66E-2	4	1.00E-4	10	1.09E-0	3
PB	70.0	10.00	4.50E-2	4	9.48E-2	3	9.46E-4	11	1.97E-2	4	4.92E-5	24	7.77E-1	3

REFERENCES

1. W.F. Baker, R.L. Cool, E.W. Jenkins, T.F. Kycia, S.J. Lindenbaum, W.A. Love, D. Lüers, J.A. Niederer, S. Ozaki, A.L. Read, J.J. Russell, and L.C. Yuan, Phys.Rev.Letters 7, 101 (1961).

2. A.N. Diddens, W. Galbraith, E. Lillethun, G. Manning, A.G. Parham, A.E. Taylor, T.G. Walker and A.M. Wetherell, Nuovo Cim. 31, 961 (1964).

3. D. Dekkers, J.A. Geibel, R. Mermod, G. Weber, T.R. Willitts, K. Winter, B. Jordan, M. Vivargent, N.M. King, and E.J.N. Wilson, Phys.Rev. 137B, 962 (1965).

4. R.A. Lundy, T.B. Novey, D.D. Yovanovitch and V.L. Telegdi, Phys.Rev.Letters 14, 504 (1965).

5. E.W. Anderson, E.J. Bleser, G.B. Collins, T. Fujii, J. Menes, F. Turkot, R.A. Carrigan, R.M. Edelstein, N.C. Hien, T.J. McMahon, and I. Nadelhaft, Phys.Rev.Letters 19, 198 (1968).

6. a) L.G. Ratner, K.W. Edwards, C.W. Akerlof, D.G. Crabb, J.L. Day, A.D. Krisch, and M.T. Lin, Phys.Rev. 166, 1353 (1968).

   b) D.G. Crabb, J.L. Day, A.D. Krisch, M.T. Lin, M.L. Marshak, J.G. Asbury, L.G. Ratner and A.L. Read, Phys.Rev.Letters 21, 830 (1968).

   c) J.G. Asbury, L.G. Ratner, A.L. Read, D.G. Crabb, J.L. Day, A.D. Krisch, M.T. Lin and M.L. Marshak, Phys.Rev.Letters 21, 1097 (1968).

   d) J.L. Day, N.P. Johnson, A.D. Krisch, M.L. Marshak, J.K. Randolph, P. Schmueser, G.J. Marmer and L.G. Ratner, Phys.Rev.Letters 23, 1055 (1969).

   e) G.J. Marmer, L.G. Ratner, J.L. Day, N.P. Johnson, P. Kalbaci, A.D. Krisch, M.L. Marshak and J.K. Randolph, Phys.Rev.Letters 23, 1469 (1969).

7. Yu.B. Bushnin, S.P. Denisov, S.V. Donskov, A.F. Dunaitsev, Yu.P. Gorin, V.A. Kachanov, Yu.S. Khodirev, V.I. Kotov, V.M. Kutyin, A.I. Petrukhin, Yu.D. Prokoshkin, E.A. Razuvaev, R.S. Shuvalov and D.A. Stoyanova;

J.V. Allaby, F. Binon, A.N. Diddens, P. Duteil, G. Giacomelli, R. Meunier, J.-P. Peigneux, K. Schlüpmann, M. Spighel, C.A. Ståhlbrandt, J.-P. Stroot and A.M. Wetherell, Phys.Letters 29B, 48 (1969) and Yadernaya Fisika 10, 585 (1969).

8. a) J.V. Allaby, F. Binon, A.N. Diddens, P. Duteil, A. Klovning, R. Meunier, J.P. Peigneux, E.J. Sacharidis, K. Schlüpmann, M. Spighel, J.P. Stroot, A.M. Thorndike, A.M. Wetherell, Phys.Letters 28B, 67 (1968).

b) Phys.Letters 28B,229 (1968).

c) Phys.Letters 29B,198 (1969).

d) Phys.Letters 30B,549 (1969).

9. L. Mazzone, CERN Internal Report MPS/Int. MU/H 68-1, 1968.

10. M. Vivargent, G. von Dardel, R. Mermod, G. Weber and K. Winter, Nuclear Instr. and Methods 22 (1963), 165.

11. P. Duteil, L. Gilly, R. Meunier, J.P. Stroot, and M. Spighel, Rev.Sci-Instr. 35, 1523 (1964).

12. V. Agoritsas, Symp. on Beam Intensity Measurements, Daresbury 1968.

13. J.B. Cumming, Ann.Rev.Nucl.Science 13, 261 (1963).

J.B. Cumming, J. Hudris, A.M. Poskanzer and S. Kauffman, Phys.Rev. 128, 2392 (1962).

14. R.F. George, K.R. Riley, R.J. Tapper, D.V. Bugg, kD.C. Salter and G.H. Stafford, Phys.Rev.Letters 15, 214 (1965).

15. R.C. Lamb, R.A. Lundy, R.B. Novey, D.D. Yovanovitch and R. Lander, Phys.Rev.Letters 17, 100 (1966).

16. G. Cocconi, D.H. Perkins and L.J. Koester, University of California Report No.UCRL-10022 (unpublished).

17. a) R. Hagedorn and J. Ranft, Suppl.Nuovo Cim. 6, 169 (1968).

b) J. Ranft, Phys.Letters 31B, 529 (1970).

18. J.R. Wayland, Phys.Rev. 175, 2106 (1968).

M. Lapointe and J.R. Wayland, Phys.Rev. 185, 2041 (1969).

19. L. Caneshi and A. Pignotti, Phys.Rev.Letters 22,1219 (1969).

FIGURE CAPTIONS

Fig. 1 Layout of the spectrometer. M. are dipole magnets; Q are quadrupole magnets; F. indicates a focus; A, S, D_1 and D_2 are scintillation counters; COLL is the collimator; SEM is the secondary emission monitor; TV indicates the beam position monitor; C_1 , C_2 and C_3 are threshold Čerenkov counters and DISC is the differential Čerenkov counter. The symbol in the quadrupole Q_1 means horizontally defocusing, that in Q_2 means horizontally focusing, etc.

Fig. 2 Ray diagram of the spectrometer. See Fig. 1 for explanation of symbols.

Fig. 3 - 8 Laboratory momentum spectrum for secondary particles produced in proton-proton collisions at 19.2 GeV/c.
Fig. 3: π^- spectra
Fig. 4: π^+ spectra
Fig. 5: K^- spectra
Fig. 6: K^+ spectra
Fig. 7: $\bar{p}$ spectra
Fig. 8: p spectra.

Fig. 9 Recapitulation of figs. 3-8.

Fig.10 Comparison of the laboratory momentum spectra for $\pi^{\pm}$, $K^{\pm}$, $p^{\pm}$, produced at 12.5 mrad by proton-proton collisions at 19.2 GeV/c.

Fig.11 Missing mass plots of the high momentum ends of the π^+ spectra at 12.5 mrad and 20 mrad laboratory production angle.

Fig.12 Region in the $\bar{p}_L$- $\bar{p}_T$ plane covered by the present experiment. The figure is actually for the case of the secondary particle being a proton, but the other 5 cases are rather similar.

Fig.13 - 18 Centre-of-momentum spectra for secondary particle production at 19.2 GeV/c. The left hand side shows the $\bar{p}_L$ dependence for fixed values of $\bar{p}_T$, the right hand side gives the $\bar{p}_T$ dependence for fixed values of $\bar{p}_L$.

Fig. 13: π^- spectra
Fig. 14: π^+ spectra
Fig. 15: K^- spectra
Fig. 16: K^+ spectra
Fig. 17: $\bar{p}$ spectra
Fig. 18: p spectra.

Fig. 19: Recapitulation of Fig. 13 - 18.

Fig. 20: Ratio of the laboratory cross-sections $d^2\sigma/d\Omega dp$ for nucleus A and for hydrogen, divided by $A^{2}/_{3}$, as a function of secondary particle momentum. The ratio is given for π^- and π^+ particles, at production angles of 12.5 and 70 mrad, for four different nuclei.

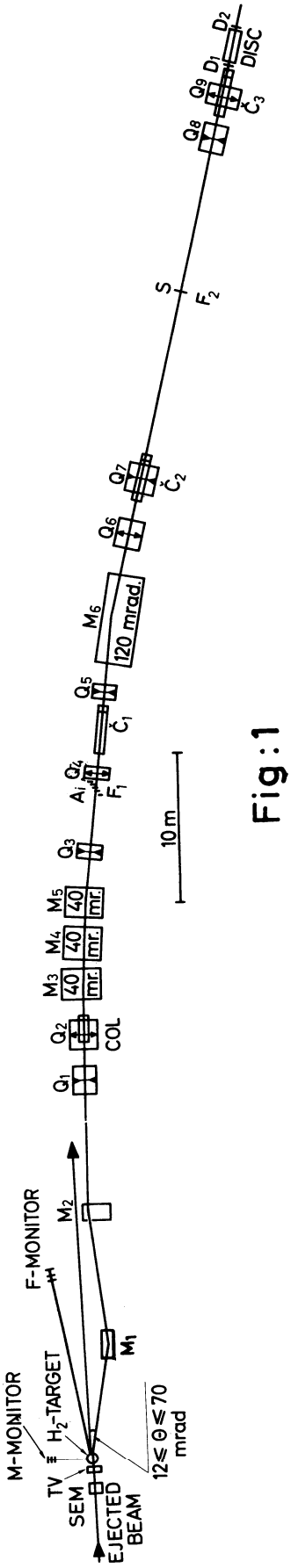
EJECTED BEAM
SEM
TV
M-MONITOR
H2-TARGET
F-MONITOR
M2
M1
12≤θ≤70 mrad
Q1
Q2
COL
M3 40 mr.
M4 40 mr.
M5 40 mr.
Q3
A1
Q4
F1
C1
Q5
M6 120 mrad.
Q6
Q7
C2
S
F2
Q8
Q9
D1
D2
DISC
C3
10 m

Fig:1

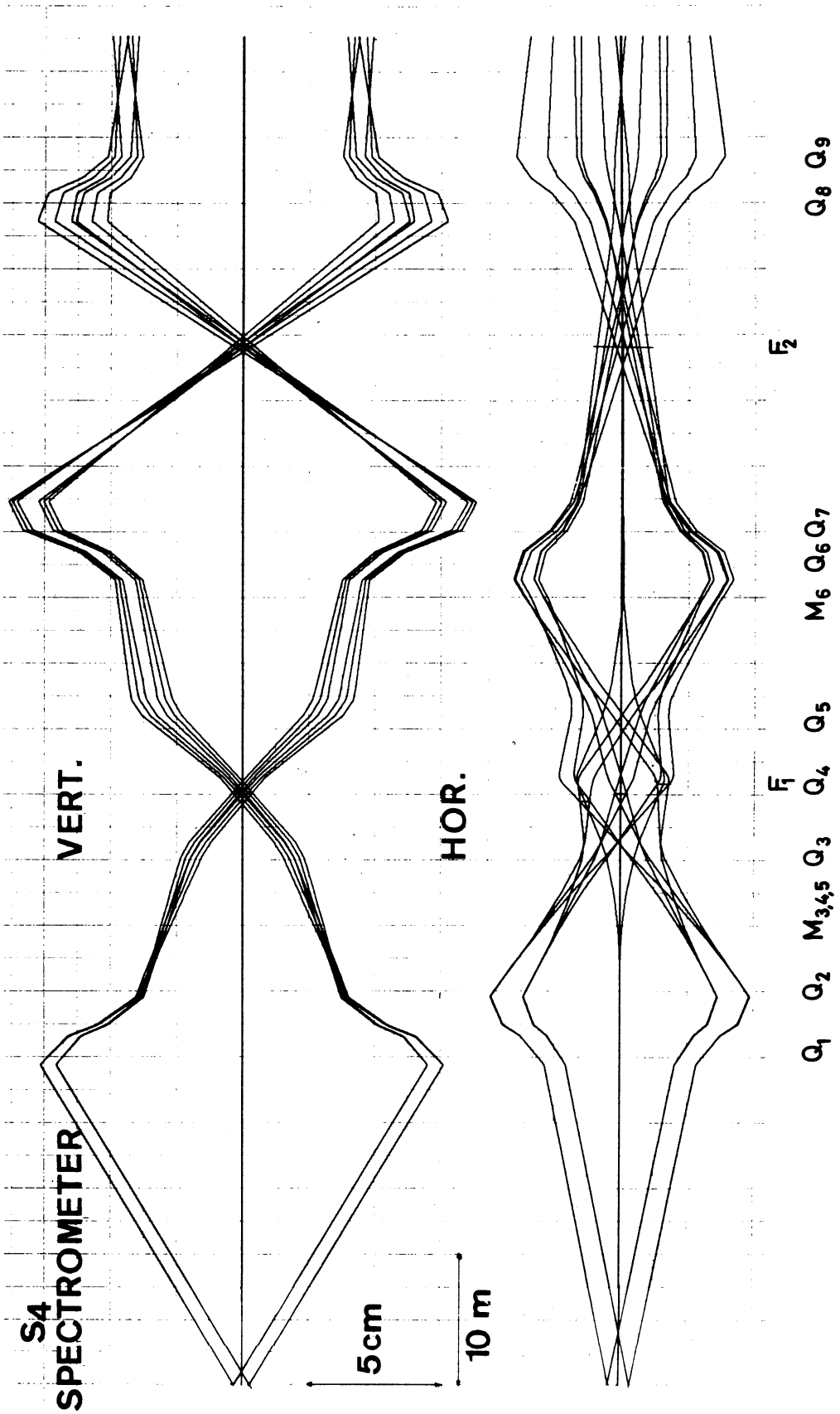
S4
SPECTROMETER
VERT.
HOR.
5cm
10 m
Q1 Q2 M3,4,5 Q3 Q4 Q5 M6 Q6 Q7 Q8 Q9
F1
F2

Fig:2

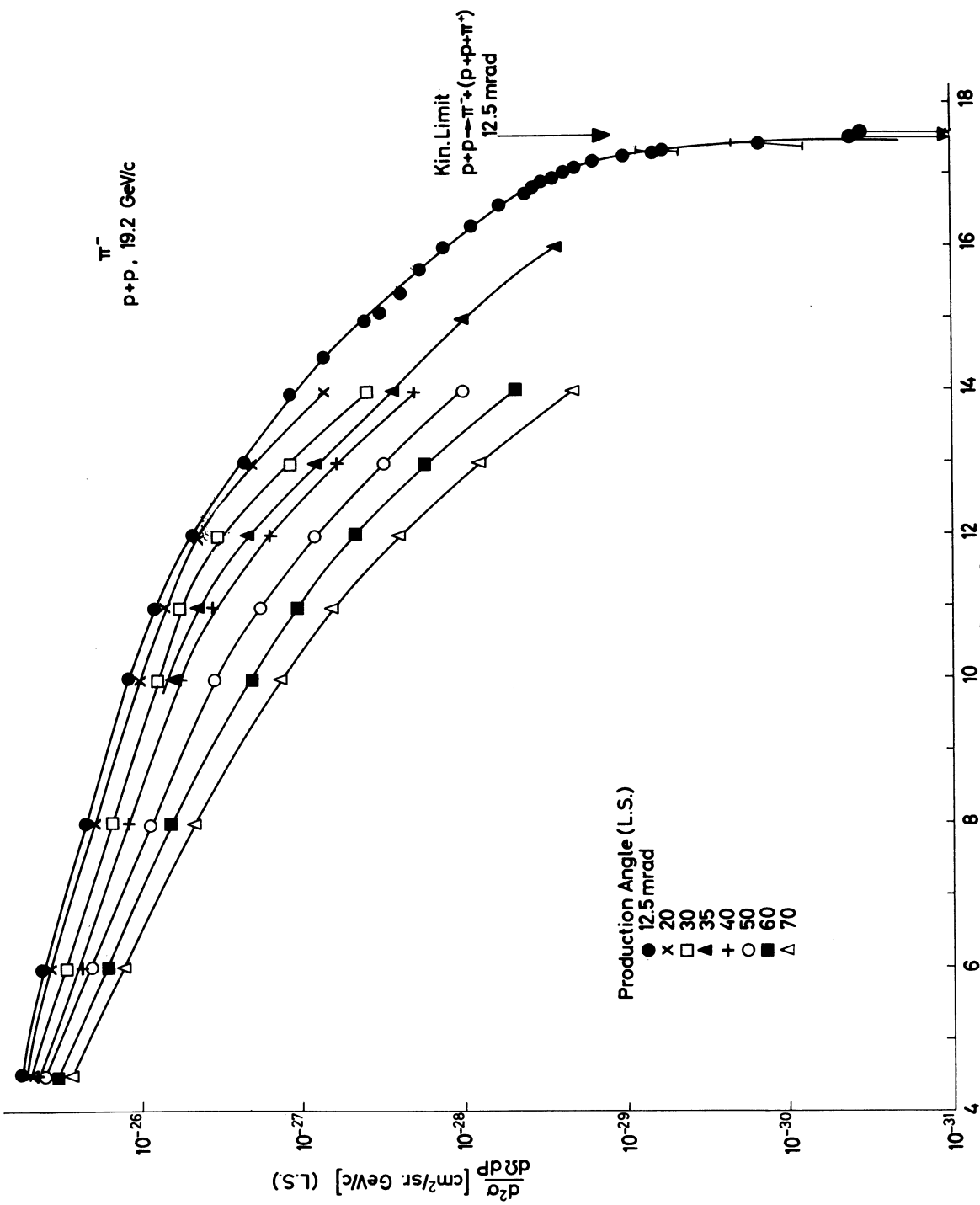
π⁻
p+p , 19.2 GeV/c
Kin.Limit
p+p→π⁻+(p+p+π⁺)
12.5 mrad
Production Angle (L.S.)
● 12.5 mrad
× 20
□ 30
◀ 35
+ 40
○ 50
■ 60
△ 70
d²σ/dΩdp [cm²/sr. GeV/c] (L.S.)
P [GeV/c]

Fig:3

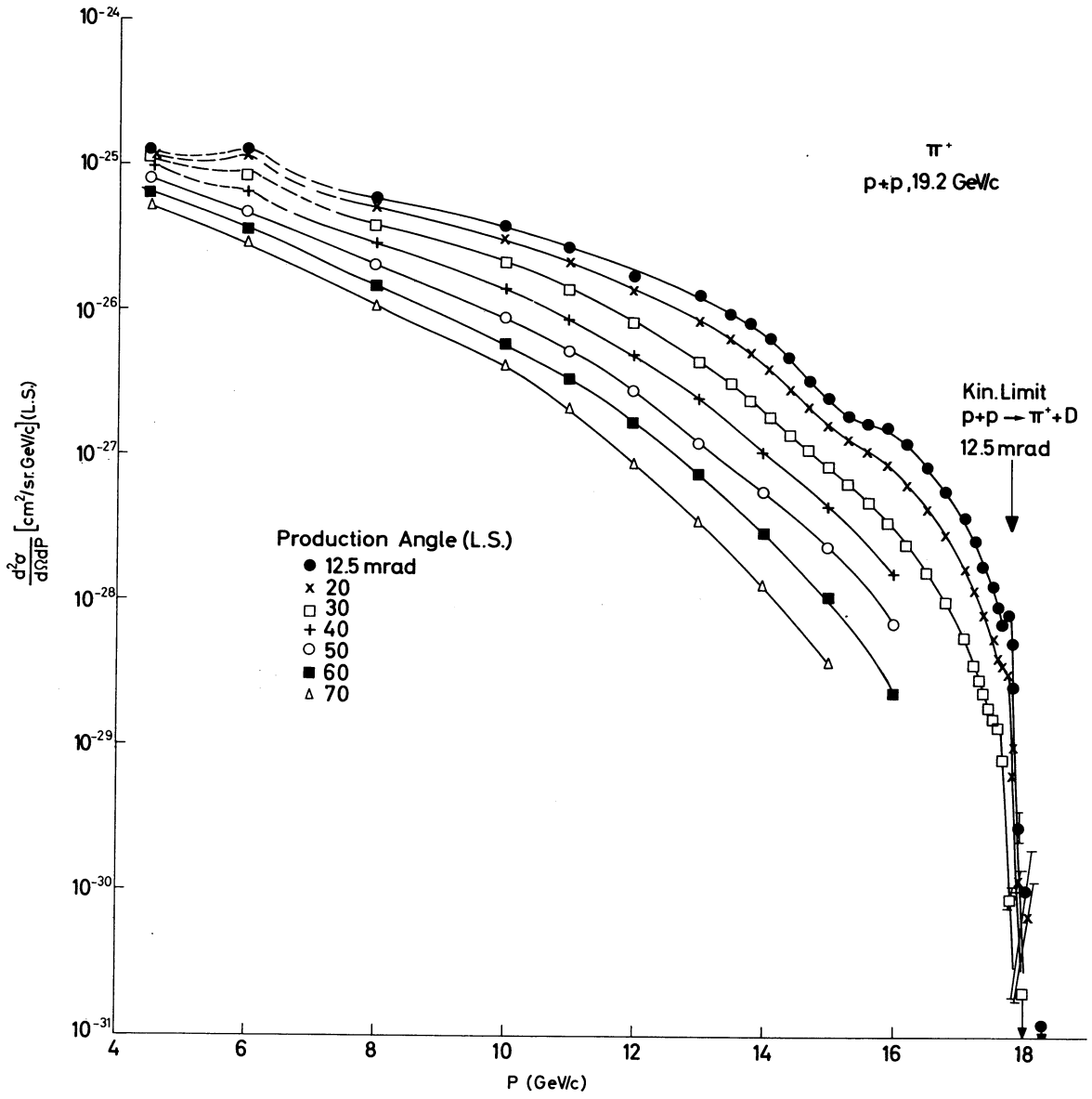
π^+
p+p, 19.2 GeV/c
Kin. Limit
p+p → π⁺+D
12.5 mrad
Production Angle (L.S.)
● 12.5 mrad
× 20
□ 30
+ 40
○ 50
■ 60
△ 70
$\frac{d^2\sigma}{d\Omega dP}$ [cm²/sr.GeV/c](L.S.)
P (GeV/c)
10⁻²⁴
10⁻²⁵
10⁻²⁶
10⁻²⁷
10⁻²⁸
10⁻²⁹
10⁻³⁰
10⁻³¹
4
6
8
10
12
14
16
18

Fig: 4

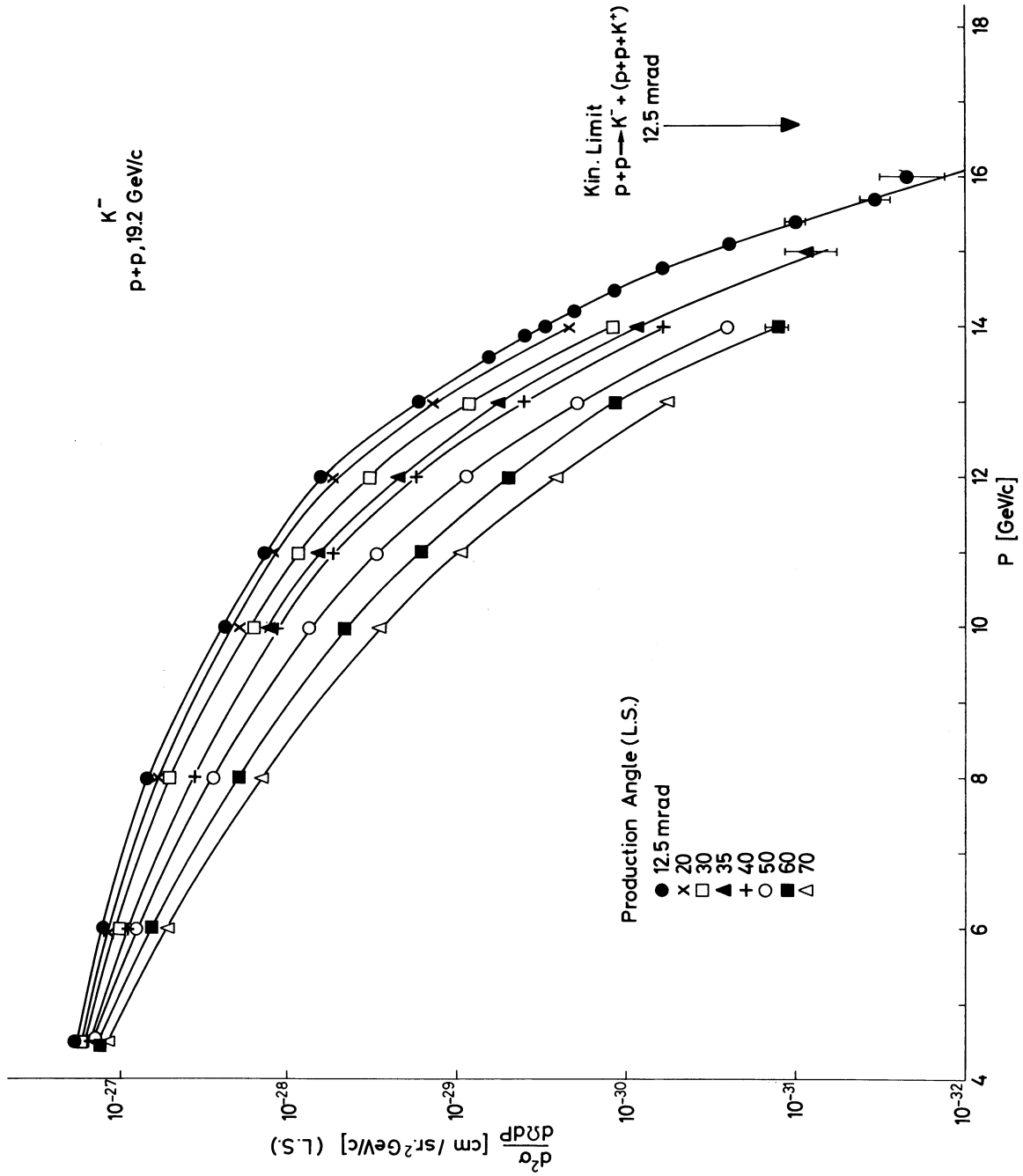
K⁻
p+p, 19.2 GeV/c
Kin. Limit
p+p→K⁻+(p+p+K⁺)
12.5 mrad
Production Angle (L.S.)
● 12.5 mrad
× 20
□ 30
▲ 35
+ 40
○ 50
■ 60
△ 70
d²σ/dΩdP [cm²/sr GeV/c] (L.S.)
P [GeV/c]

Fig:5

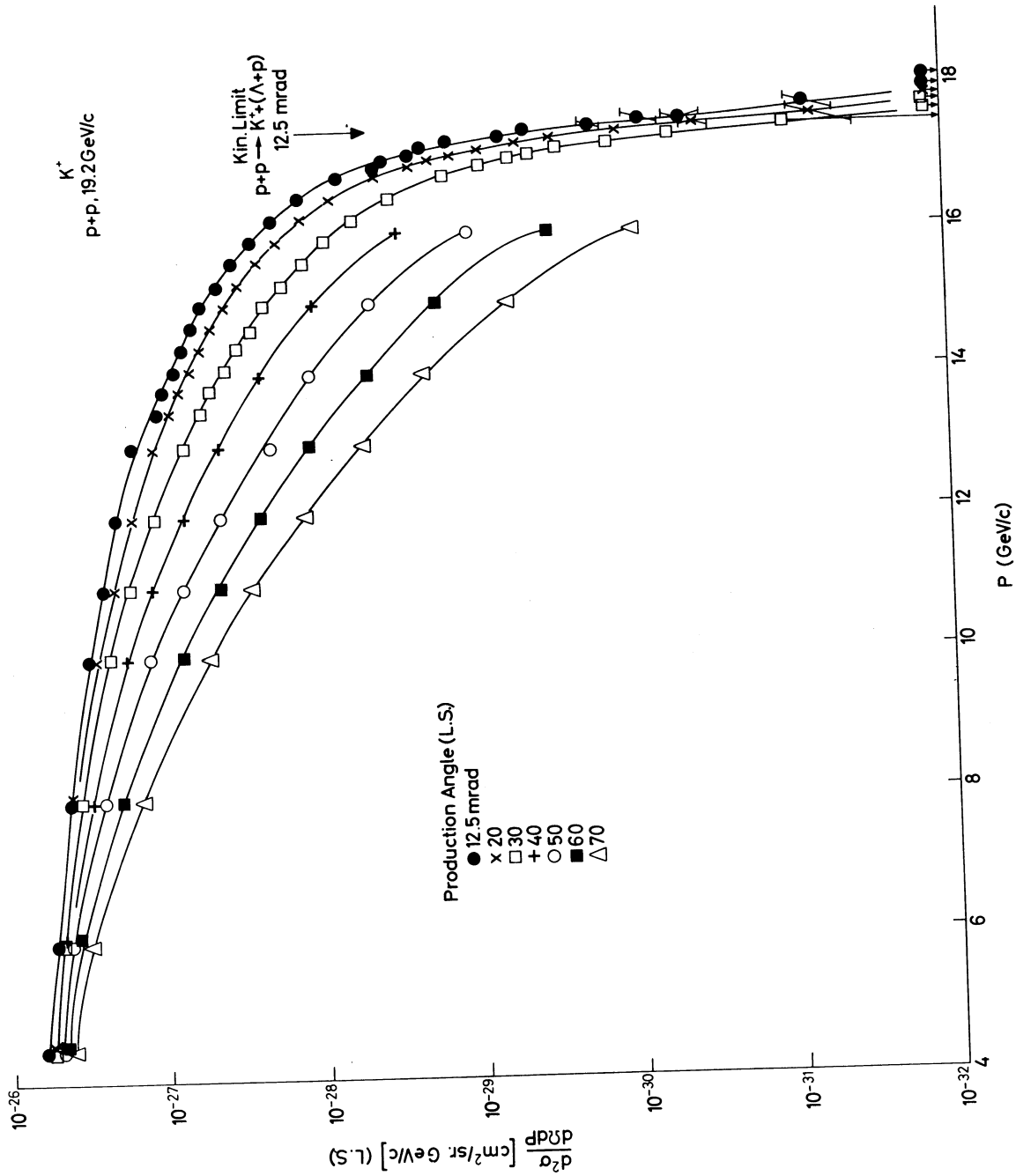
K+
p+p, 19.2 GeV/c
Kin. Limit
p+p → K+(Λ+p)
12.5 mrad
Production Angle (L.S.)
● 12.5 mrad
x 20
□ 30
+ 40
○ 50
■ 60
△ 70
d²σ/dΩdP [cm²/sr. GeV/c] (L.S.)
P (GeV/c)

Fig:6

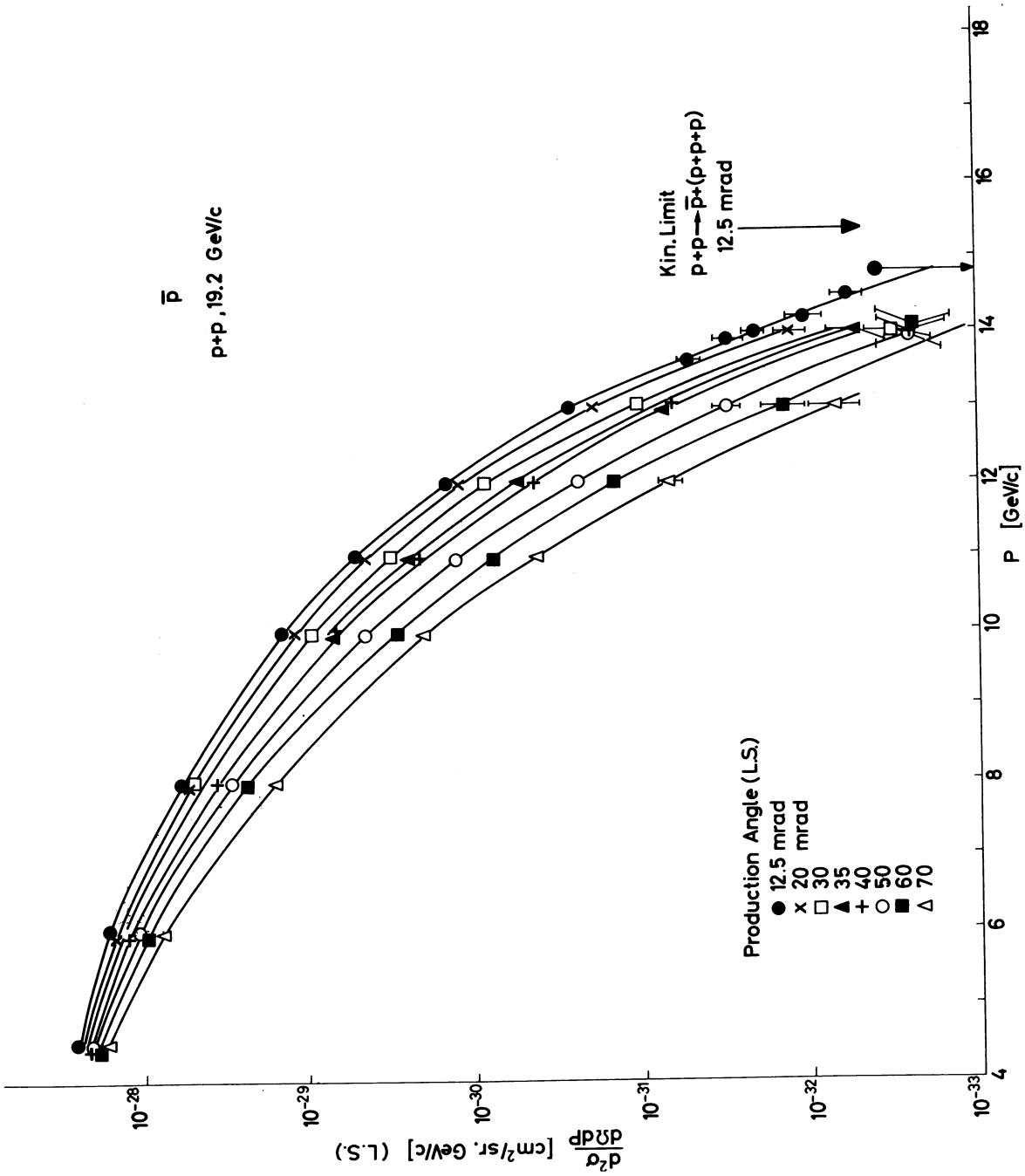
p̄
p+p, 19.2 GeV/c
Kin. Limit
p+p→p̄+(p+p+p)
12.5 mrad
Production Angle (L.S.)
● 12.5 mrad
× □ 20 mrad
□ 30
▲ 35
+ ○ 40
○ 50
■ 60
△ 70
d²σ/dΩdp [cm²/sr. GeV/c] (L.S.)
P [GeV/c]

Fig:7

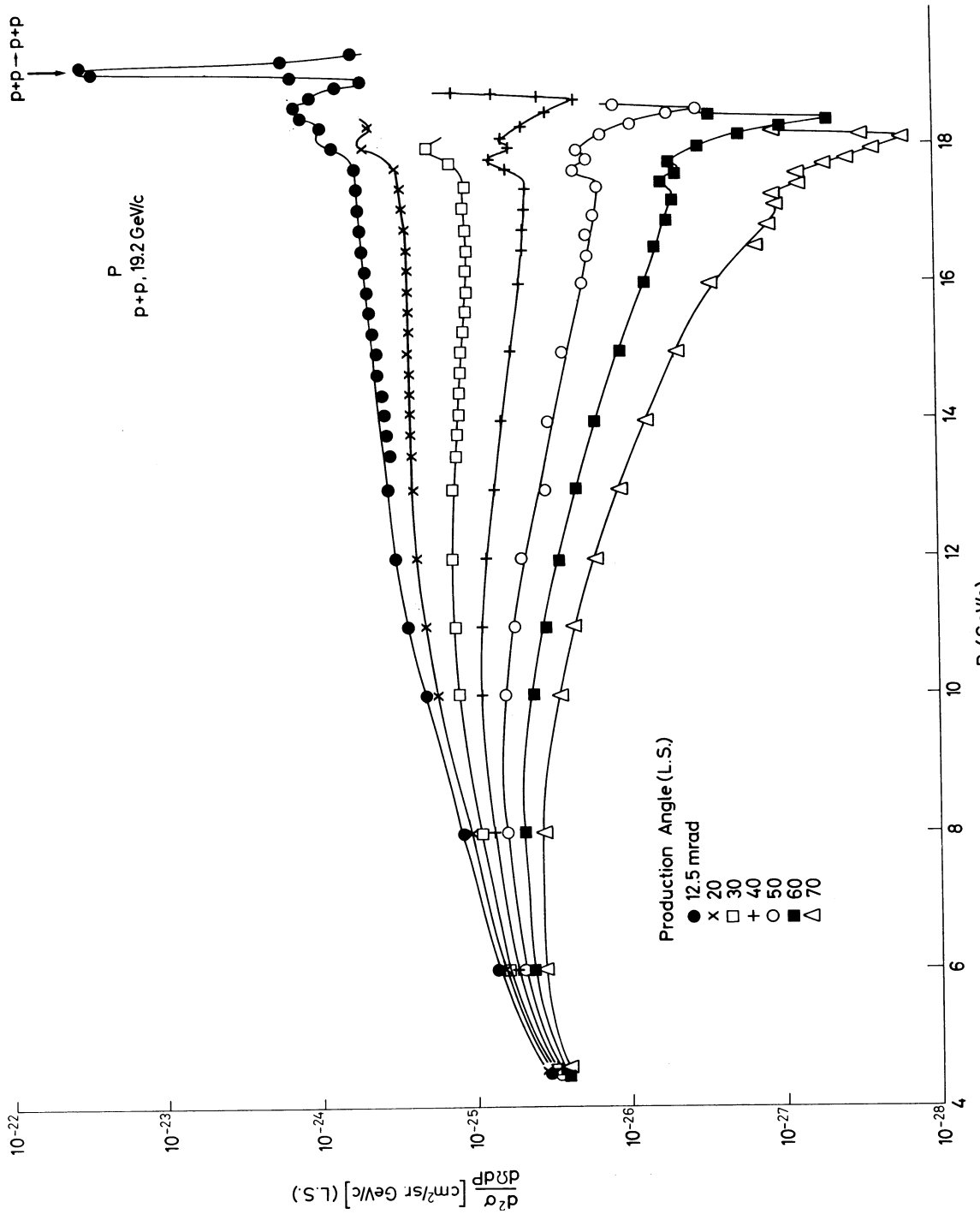
p+p → p+p
P
p+p, 19.2 GeV/c
Production Angle (L.S.)
● 12.5 mrad
× 20
□ 30
+ 40
○ 50
■ 60
△ 70
$\frac{d^2\sigma}{d\Omega dP}$ [cm²/sr GeV/c] (L.S.)
P (GeV/c)
10⁻²²
10⁻²³
10⁻²⁴
10⁻²⁵
10⁻²⁶
10⁻²⁷
10⁻²⁸
4
6
8
10
12
14
16
18

Fig:8

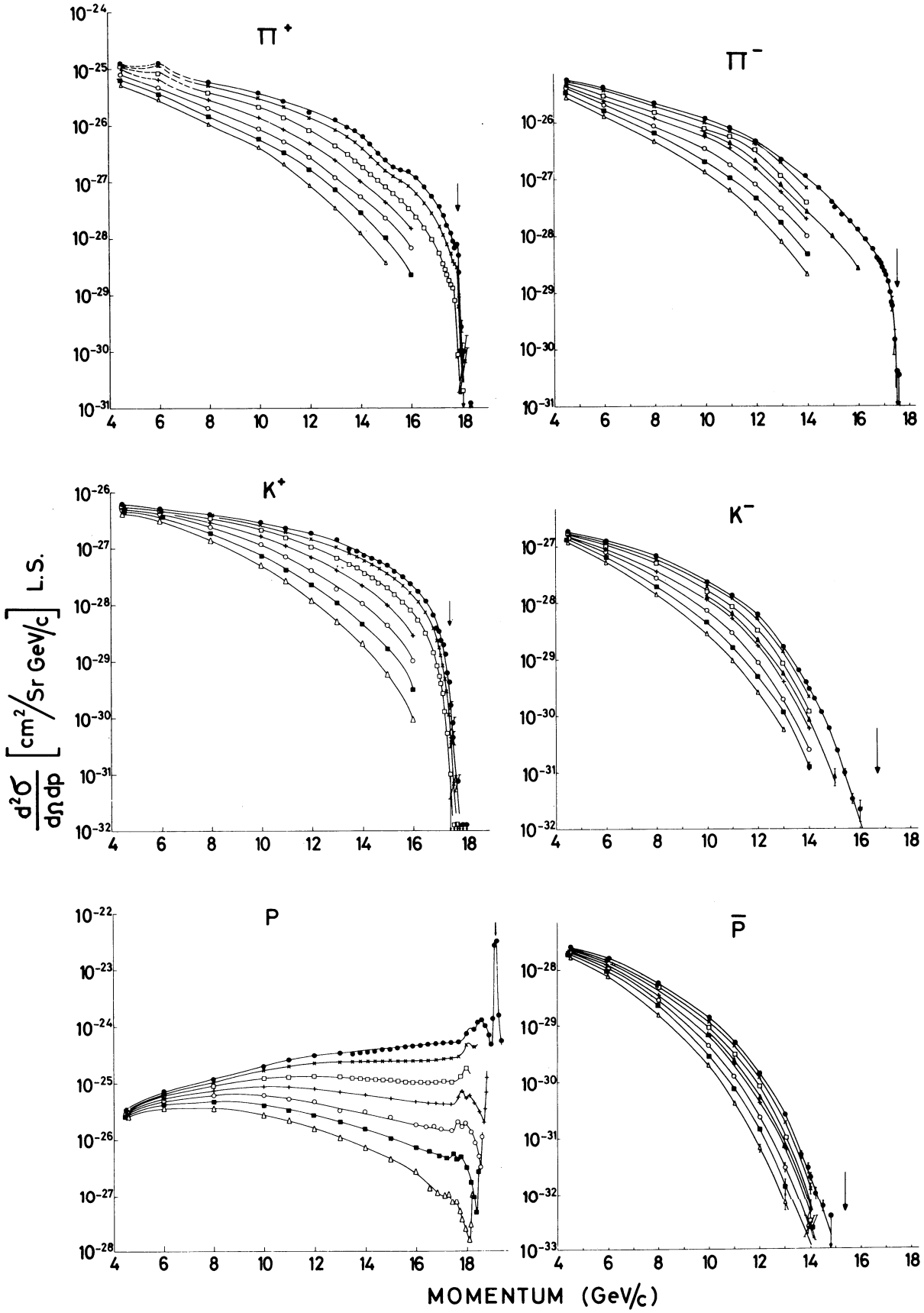

Fig:9

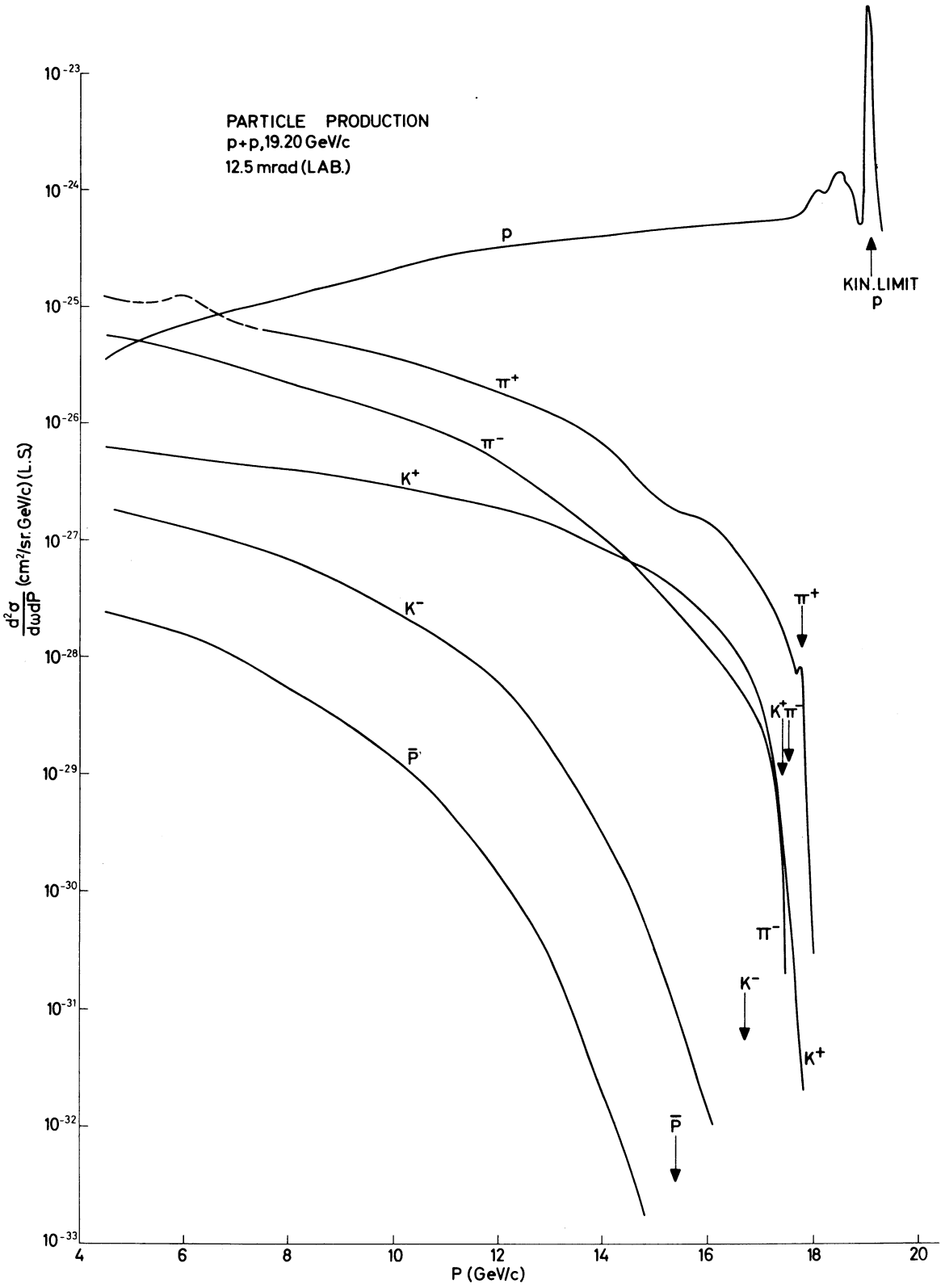
PARTICLE PRODUCTION
p+p, 19.20 GeV/c
12.5 mrad (LAB.)
p
KIN. LIMIT p
π+
π−
K+
K−
P̄
π+
K+π−
π−
K−
K+
P̄
$\frac{d^2\sigma}{d\omega dP}$ (cm²/sr.GeV/c) (L.S)
P (GeV/c)

Fig:10

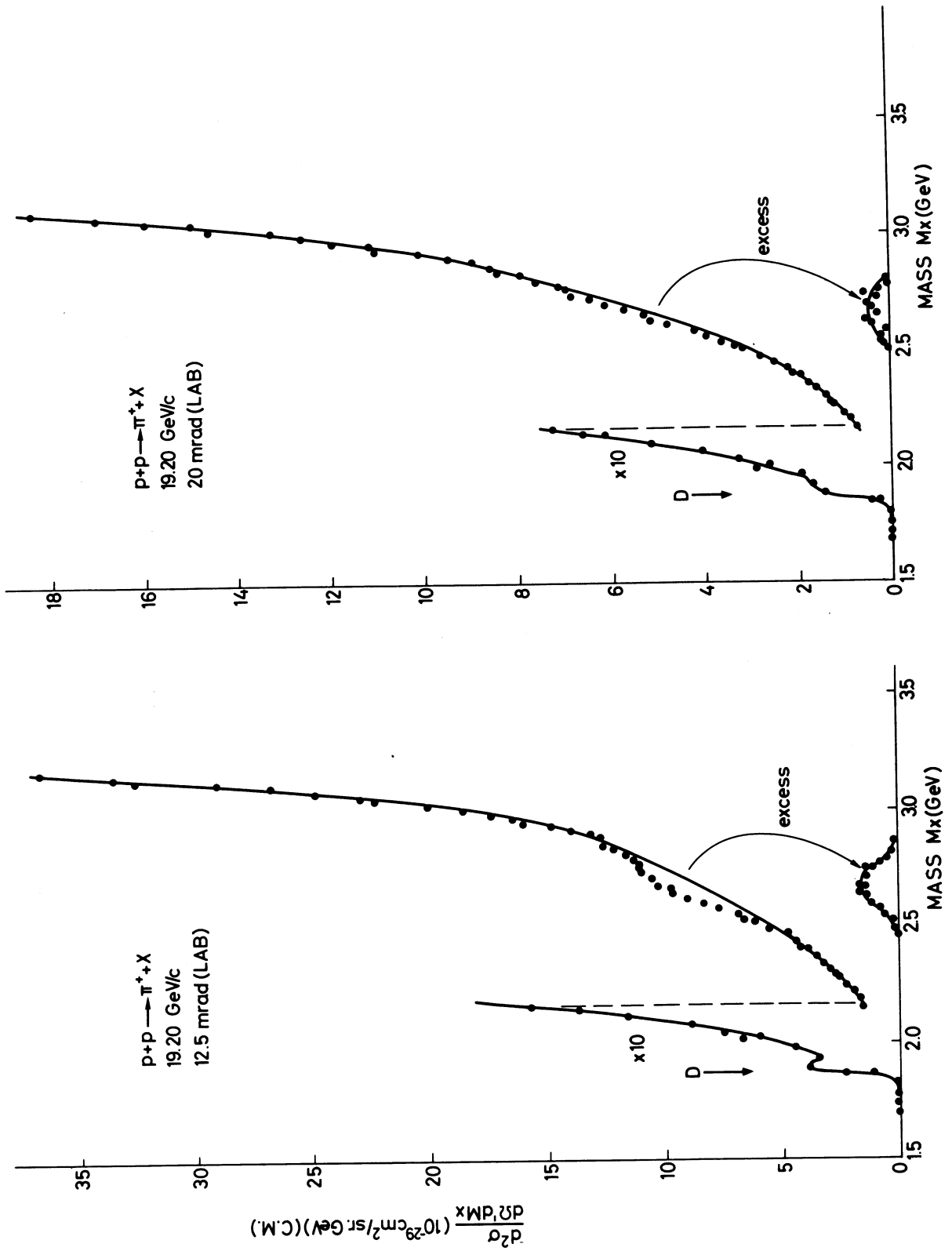
p+p→π⁺+X
19.20 GeV/c
12.5 mrad (LAB)
p+p→π⁺+X
19.20 GeV/c
20 mrad (LAB)
x10
D
excess
MASS Mx(GeV)
d²σ/dΩ'dMx (10⁻²⁹cm²/sr.GeV)(C.M.)

Fig:11

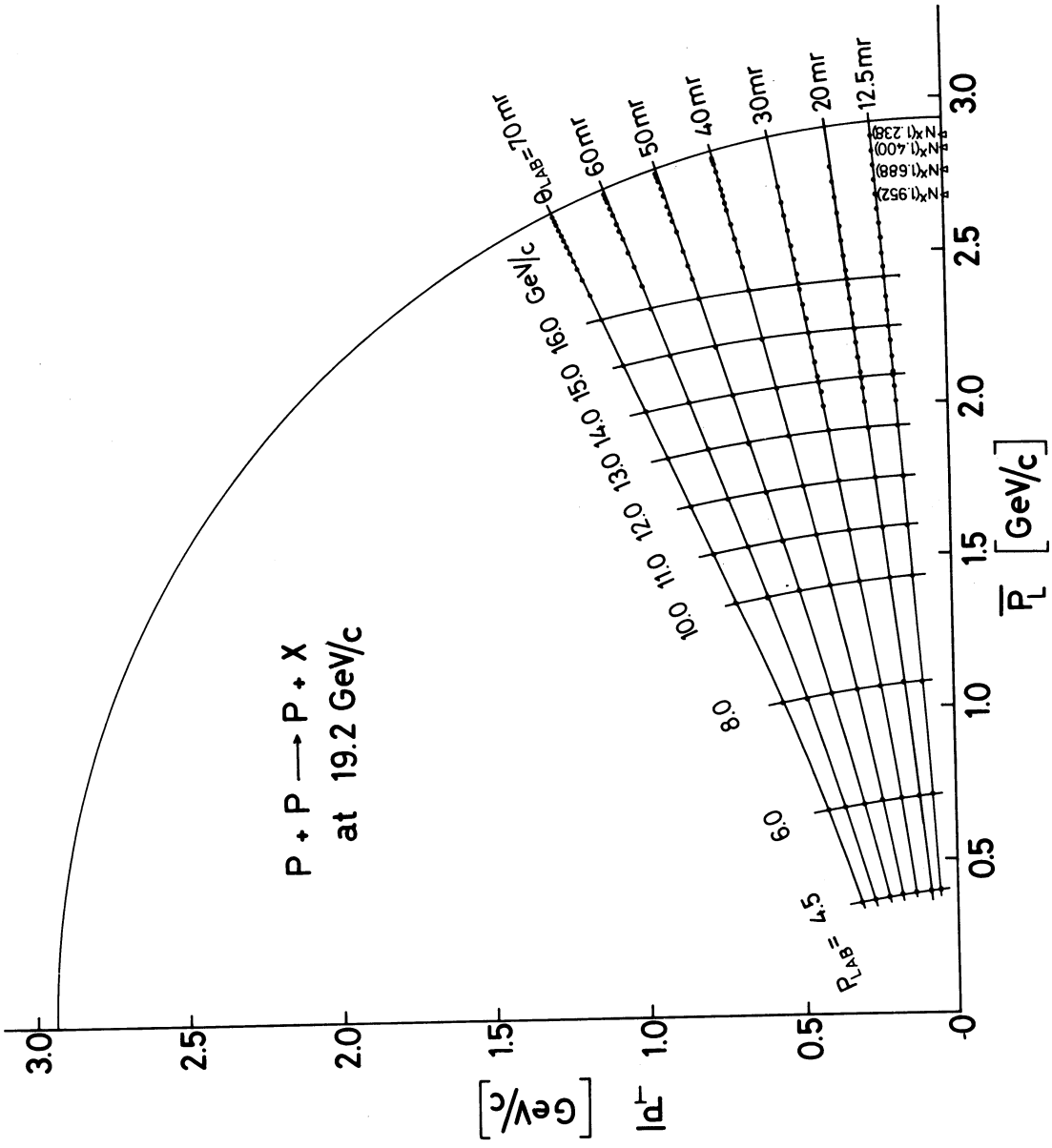
P + P ⟶ P + X
at 19.2 GeV/c
θ_{LAB}=70mr
60mr
50mr
40mr
30mr
20mr
12.5mr
R_{LAB}= 4.5
6.0
8.0
10.0
11.0
12.0
13.0
14.0
15.0
16.0 GeV/c
p_T [GeV/c]
$\overline{p}_L$ [GeV/c]
0
0.5
1.0
1.5
2.0
2.5
3.0

Fig:12

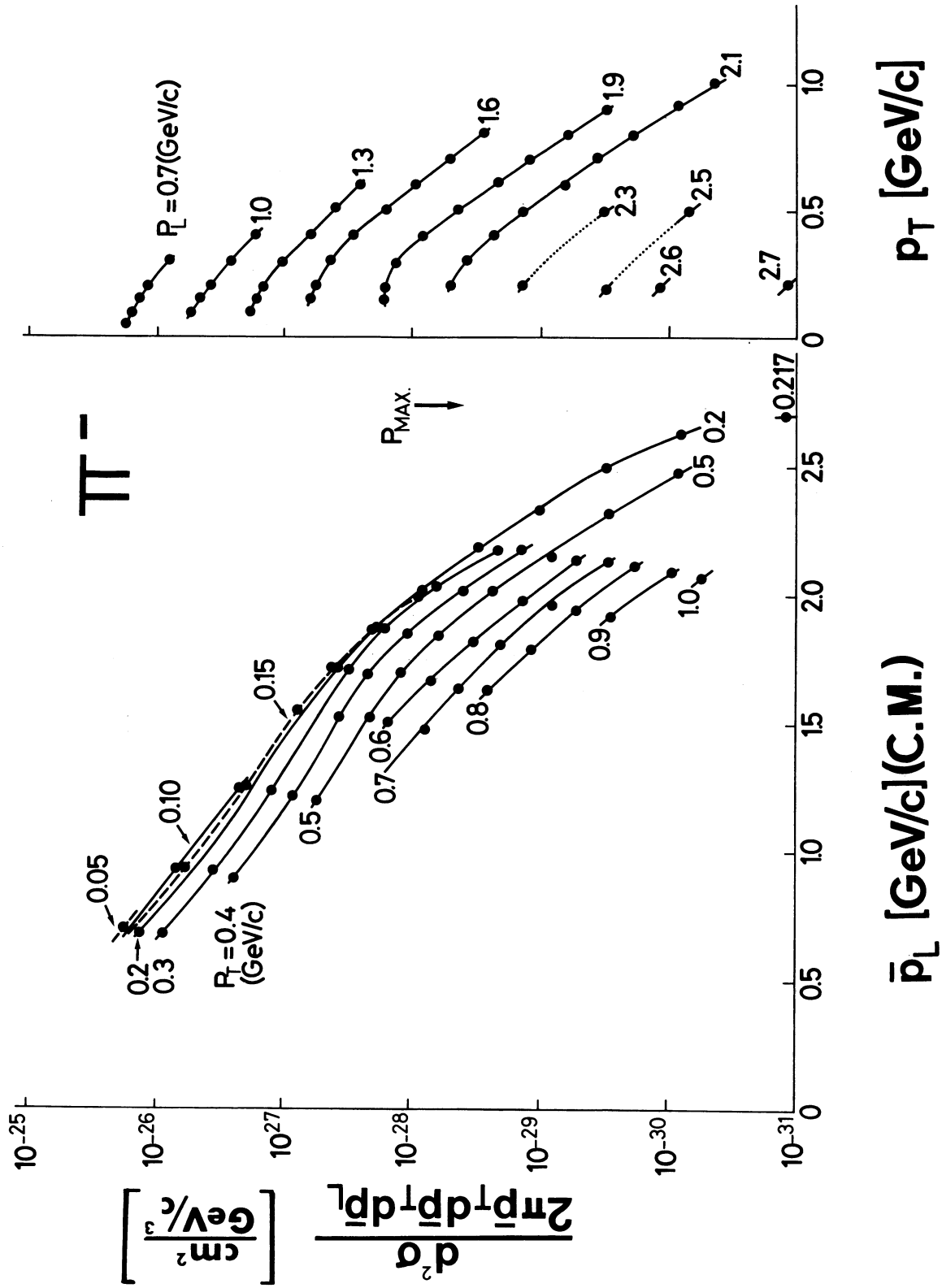
π^-
P_L=0.7(GeV/c)
1.0
1.3
1.6
1.9
2.1
2.3
2.5
2.6
2.7
$P_{MAX.}$
0.217
P_T=0.4 (GeV/c)
0.05
0.10
0.15
0.2
0.3
0.5
0.6
0.7
0.8
0.9
1.0
$\frac{d^2\sigma}{2\pi p_T dp_T dp_L}$ $\left[\frac{cm^2}{GeV/c^2}\right]$
$\bar{p}_L$ [GeV/c](C.M.)
p_T [GeV/c]

Fig:13

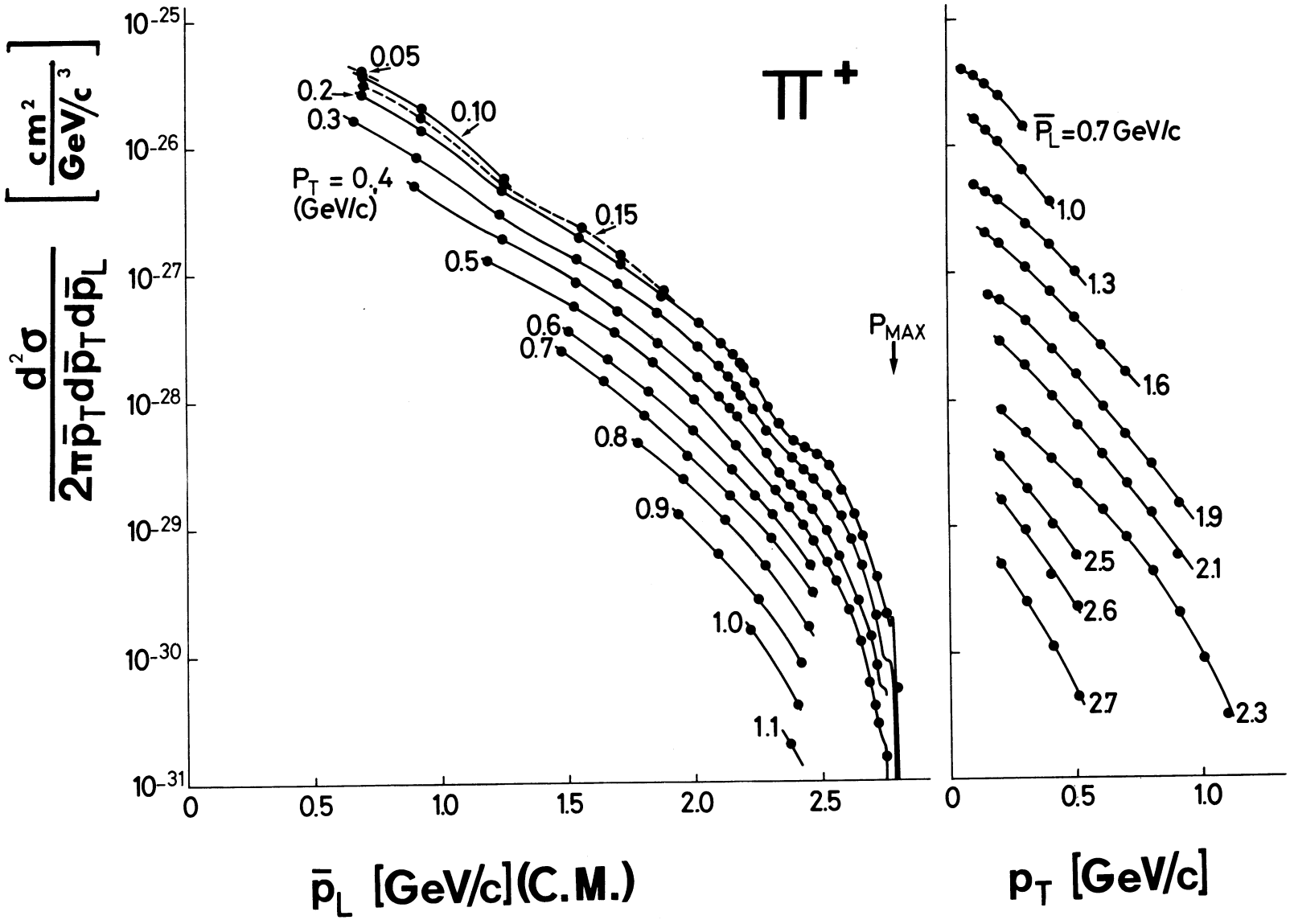
$\frac{d^2\sigma}{2\pi \bar{p}_T d\bar{p}_T d\bar{p}_L}$ $\left[\frac{cm^2}{GeV/c^3}\right]$
10^{-25}
10^{-26}
10^{-27}
10^{-28}
10^{-29}
10^{-30}
10^{-31}
π^+
0.05
0.2
0.3
0.10
P_T = 0.4 (GeV/c)
0.15
0.5
0.6
0.7
0.8
0.9
1.0
1.1
P_{MAX}
$\bar{P}_L$=0.7 GeV/c
1.0
1.3
1.6
1.9
2.1
2.3
2.5
2.6
2.7
0
0.5
1.0
1.5
2.0
2.5
$\bar{p}_L$ [GeV/c](C.M.)
p_T [GeV/c]

Fig:14

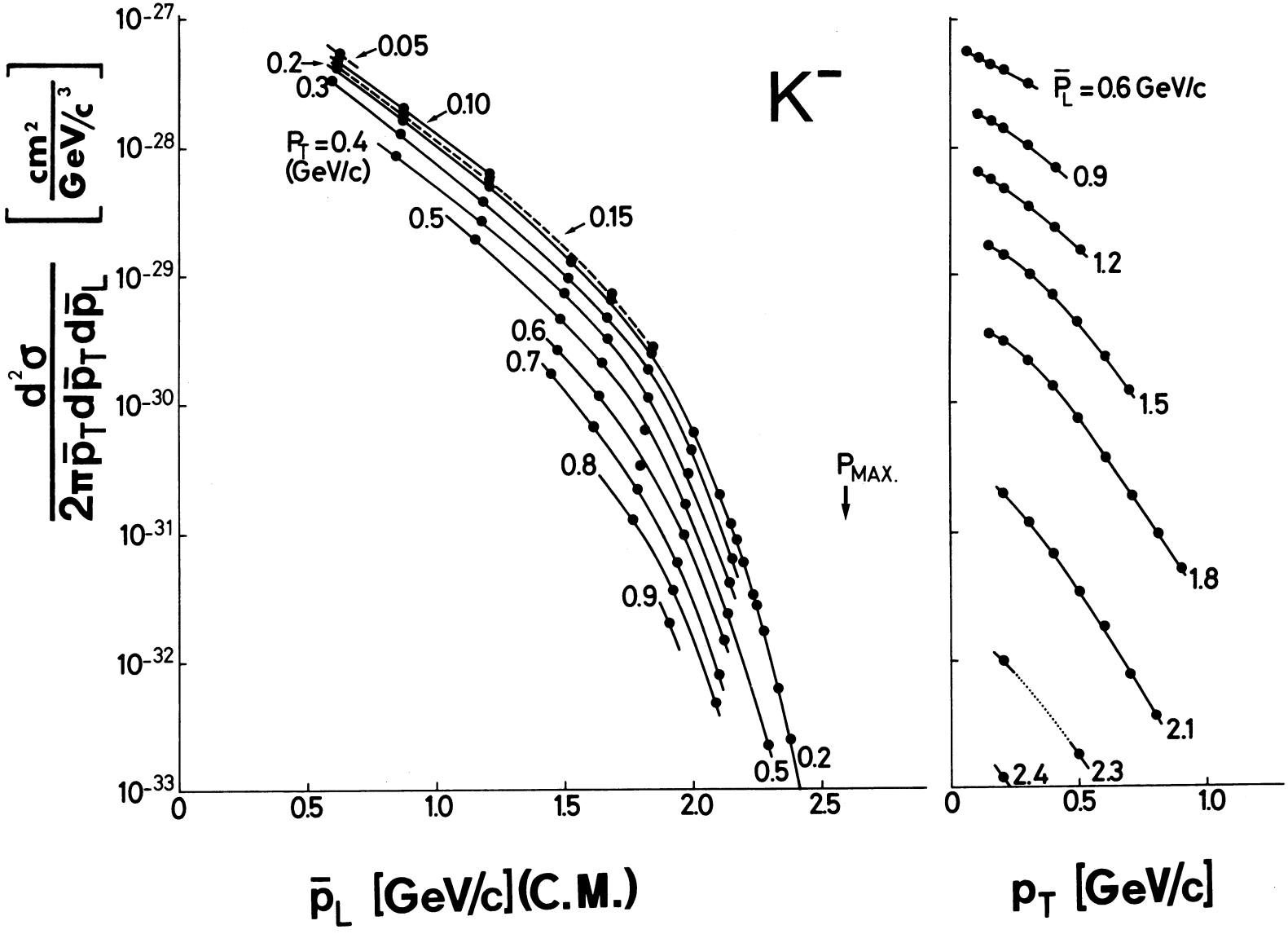
$\frac{d^2\sigma}{2\pi \bar{p}_T d\bar{p}_T d\bar{p}_L}$ $\left[\frac{cm^2}{GeV/c^3}\right]$
10^{-27}
10^{-28}
10^{-29}
10^{-30}
10^{-31}
10^{-32}
10^{-33}
0
0.5
1.0
1.5
2.0
2.5
K^-
$P_T = 0.4$ (GeV/c)
0.05
0.10
0.15
0.2
0.3
0.5
0.6
0.7
0.8
0.9
0.5
0.2
$P_{MAX.}$
$\bar{p}_L$ [GeV/c](C.M.)
$\bar{P}_L = 0.6$ GeV/c
0.9
1.2
1.5
1.8
2.1
2.3
2.4
0
0.5
1.0
p_T [GeV/c]

Fig: 15

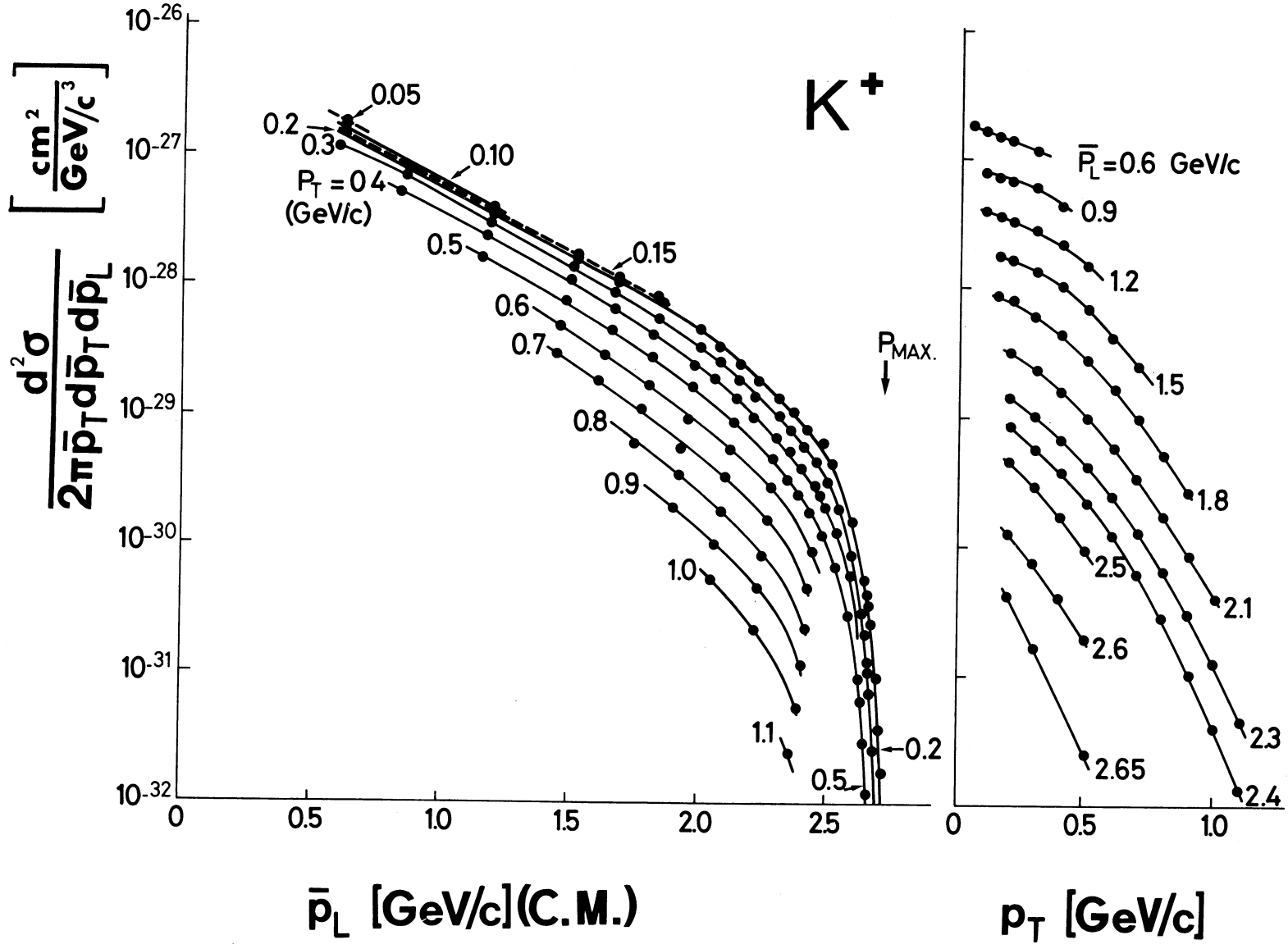
$\frac{d^2\sigma}{2\pi \bar{p}_T d\bar{p}_T d\bar{p}_L}$ $\left[\frac{cm^2}{GeV/c^3}\right]$
10^{-26}
10^{-27}
10^{-28}
10^{-29}
10^{-30}
10^{-31}
10^{-32}
0
0.5
1.0
1.5
2.0
2.5
K^+
0.05
0.2
0.3
0.10
P_T = 0.4 (GeV/c)
0.5
0.15
0.6
0.7
0.8
0.9
1.0
1.1
0.5
0.2
$P_{MAX.}$
$\bar{P}_L$=0.6 GeV/c
0.9
1.2
1.5
1.8
2.1
2.3
2.4
2.65
2.6
2.5
0
0.5
1.0
$\bar{p}_L$ [GeV/c](C.M.)
p_T [GeV/c]

Fig:16

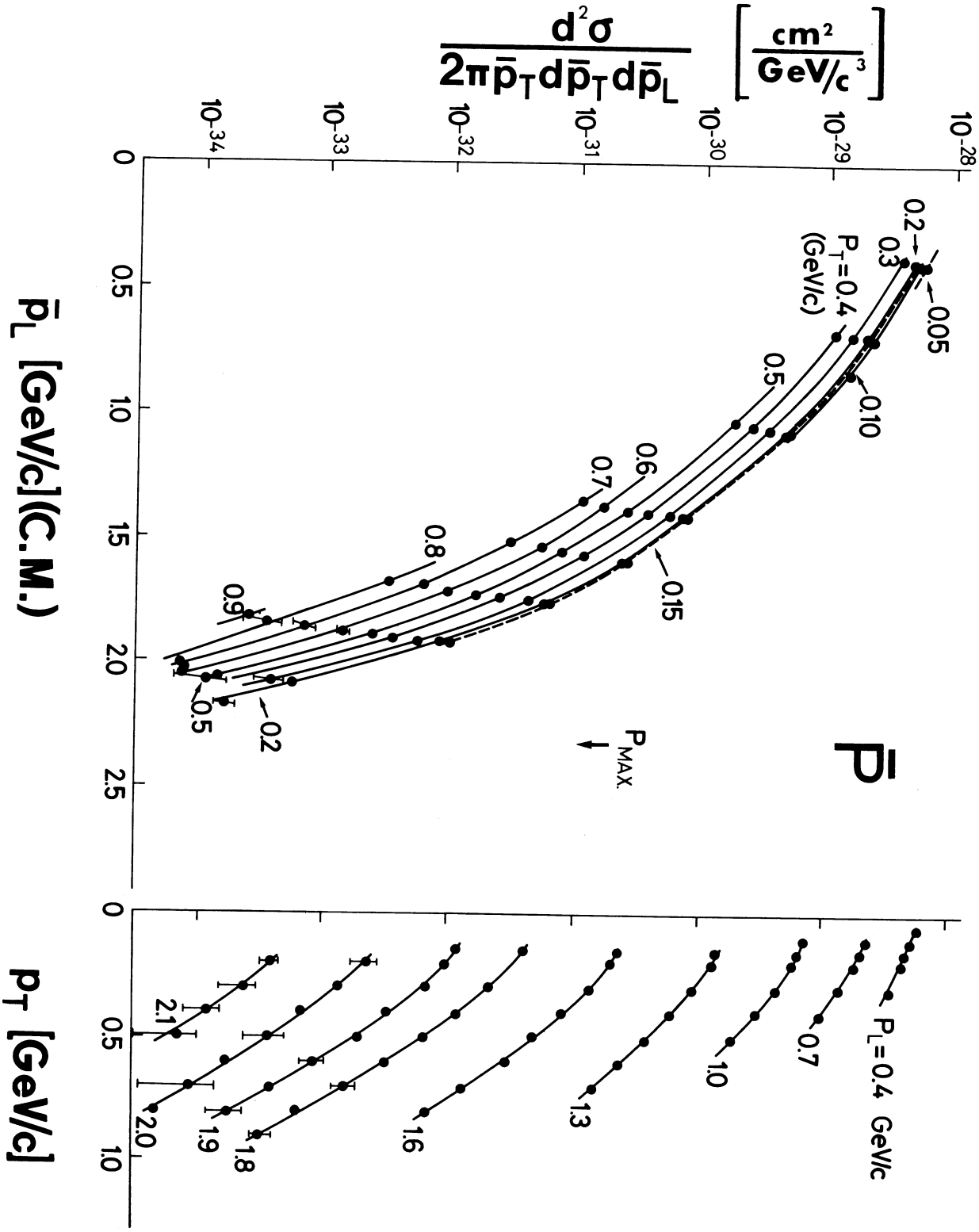
$\frac{d^2\sigma}{2\pi \bar{p}_T d\bar{p}_T d\bar{p}_L}$ $\left[\frac{cm^2}{GeV/c^3}\right]$
10^{-28}
10^{-29}
10^{-30}
10^{-31}
10^{-32}
10^{-33}
10^{-34}
$\bar{p}$
$P_{MAX.}$
P_T=0.4 (GeV/c)
0.2
0.3
0.05
0.10
0.5
0.6
0.7
0.8
0.9
0.15
0.5
0.2
0
0.5
1.0
1.5
2.0
2.5
$\bar{p}_L$ [GeV/c](C.M.)
P_L=0.4 GeV/c
0.7
1.0
1.3
1.6
1.8
1.9
2.0
2.1
0
0.5
1.0
p_T [GeV/c]

Fig:17

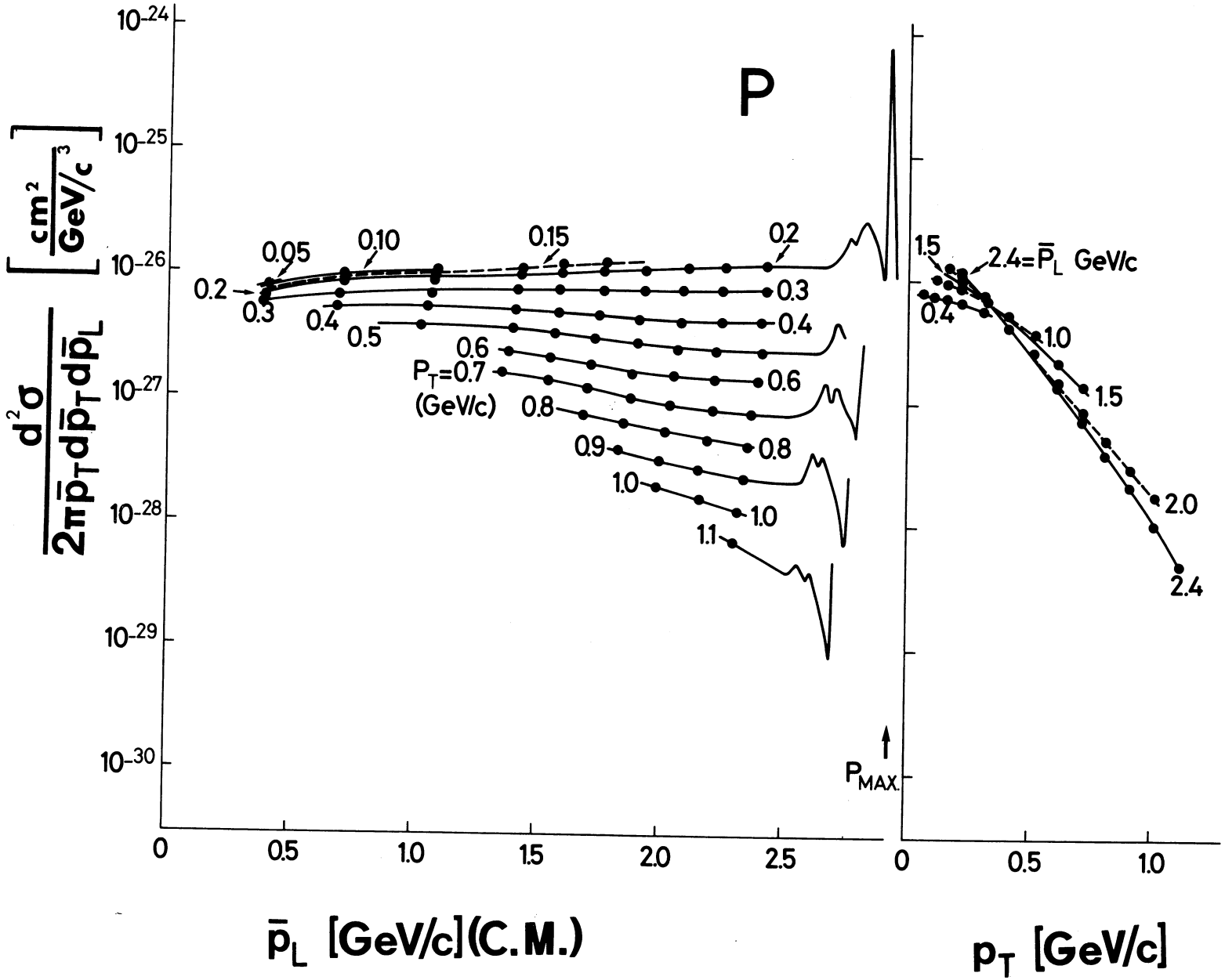
P
$\frac{d^2\sigma}{2\pi \bar{p}_T d\bar{p}_T d\bar{p}_L}$ $\left[\frac{cm^2}{GeV/c^3}\right]$
10^{-24}
10^{-25}
10^{-26}
10^{-27}
10^{-28}
10^{-29}
10^{-30}
0.05
0.10
0.15
0.2
0.2
0.3
0.3
0.4
0.4
0.5
0.6
P_T=0.7
(GeV/c)
0.6
0.8
0.8
0.9
1.0
1.0
1.1
$P_{MAX.}$
0
0.5
1.0
1.5
2.0
2.5
$\bar{p}_L$ [GeV/c](C.M.)
1.5
2.4=$\bar{P}_L$ GeV/c
0.4
1.0
1.5
2.0
2.4
0
0.5
1.0
p_T [GeV/c]

Fig:18

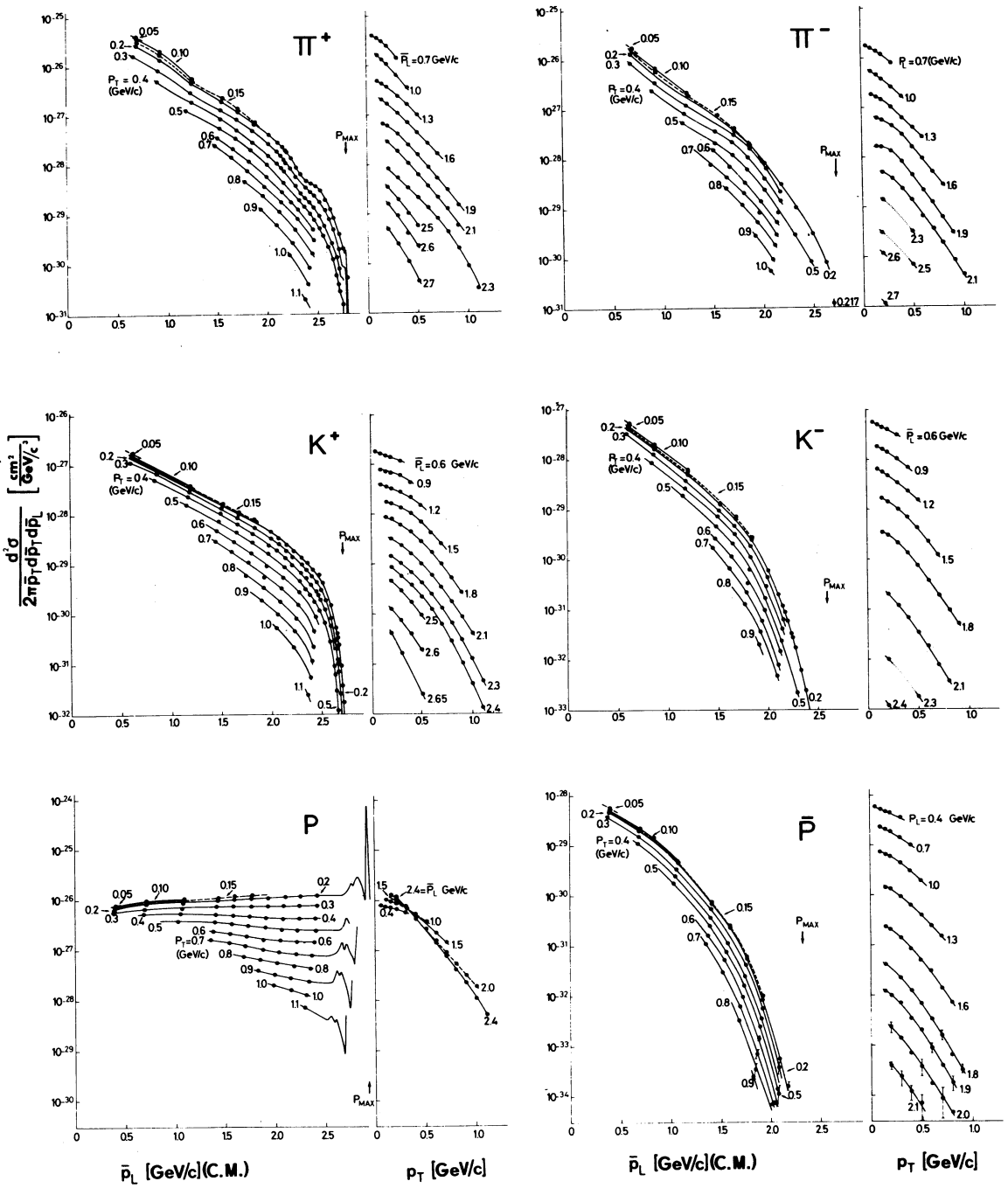
π+
π-
K+
K-
P
P̄
P_T = 0.4 (GeV/c)
P_T=0.7 (GeV/c)
P_L=0.7 GeV/c
P_L=0.6 GeV/c
P_L=0.4 GeV/c
P_L=2.4=P̄_L GeV/c
P_MAX
+0.217
d²σ / 2πp̄_T dp̄_T dp̄_L [cm²/GeV/c²]
p̄_L [GeV/c](C.M.)
p_T [GeV/c]

Fig:19

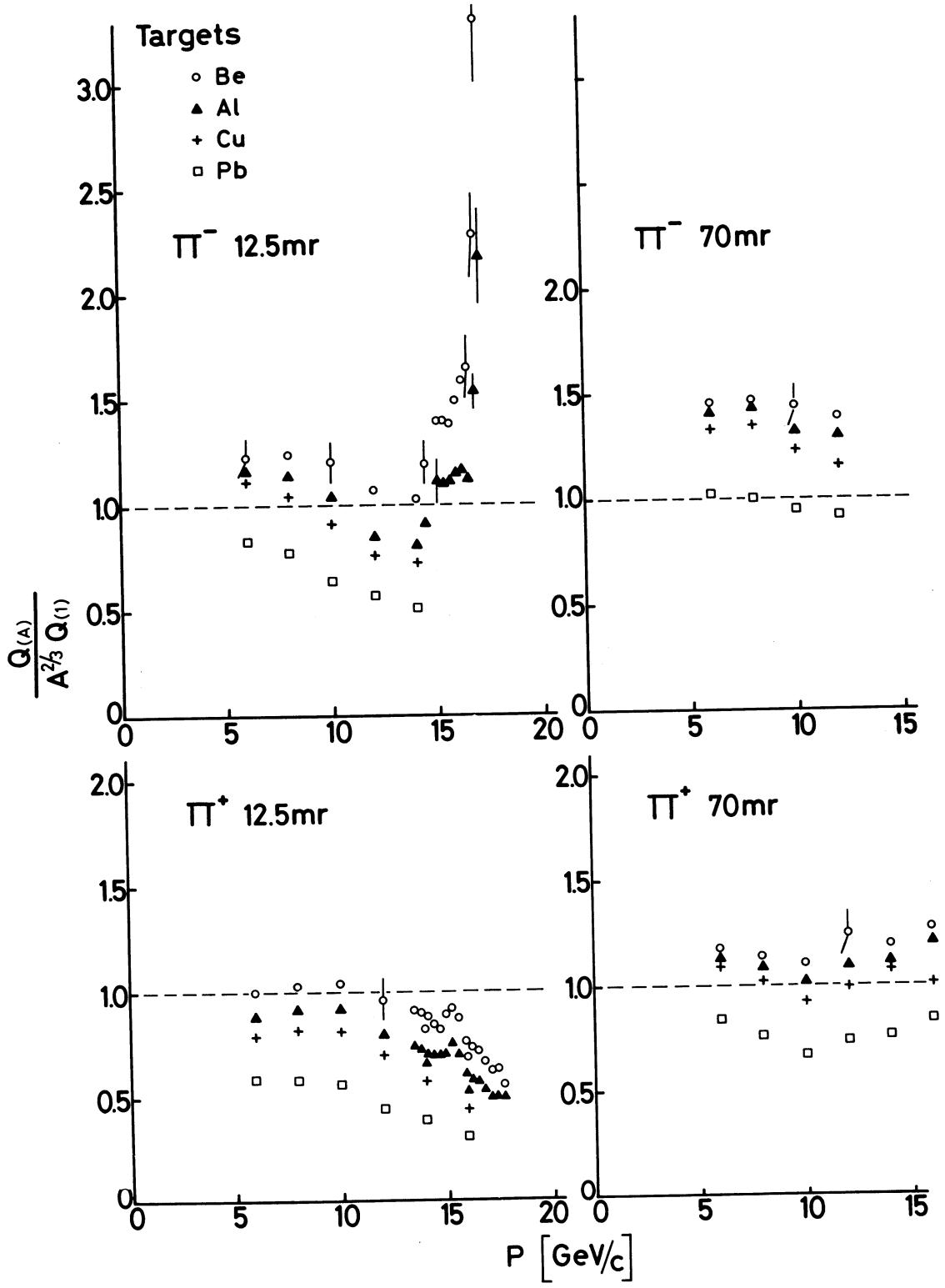
Targets
Be
Al
Cu
Pb
TT⁻ 12.5mr
TT⁻ 70mr
TT⁺ 12.5mr
TT⁺ 70mr
Q(A) / A^2/3 Q(1)
P [GeV/c]

Fig:20